Journal of Chromatography A, 1218 (2011) 1153–1169

Contents lists available at ScienceDirect

Journal of Chromatography A

journal homepage: www.elsevier.com/locate/chroma

# Kinetic performance limits of constant pressure versus constant flow rate gradient elution separations. Part I: Theory

K. Broeckhoven[a], M. Verstraeten[a], K. Choikhet[b], M. Dittmann[b], K. Witt[b], G. Desmet[a,*]

[a] Vrije Universiteit Brussel, Department of Chemical Engineering (CHIS-IR), Pleinlaan 2, 1050 Brussels, Belgium
[b] Agilent Technologies Germany GmbH, Hewlett-Packard Str. 8, Waldbronn BW 76337, Germany

ARTICLE INFO

*Article history:*
Received 4 October 2010
Received in revised form
16 December 2010
Accepted 19 December 2010
Available online 28 December 2010

*Keywords:*
Constant pressure
Kinetic plot method
Peak capacity
Plate height
Numerical simulation
Pressure effects

ABSTRACT

We report on a general theoretical assessment of the potential kinetic advantages of running LC gradient elution separations in the constant-pressure mode instead of in the customarily used constant-flow rate mode. Analytical calculations as well as numerical simulation results are presented. It is shown that, provided both modes are run with the same volume-based gradient program, the constant-pressure mode can potentially offer an identical separation selectivity (except from some small differences induced by the difference in pressure and viscous heating trajectory), but in a significantly shorter time. For a gradient running between 5 and 95% of organic modifier, the decrease in analysis time can be expected to be of the order of some 20% for both water–methanol and water–acetonitrile gradients, and only weakly depending on the value of $V_G/V_0$ (or equivalently $t_G/t_0$). Obviously, the gain will be smaller when the start and end composition lie closer to the viscosity maximum of the considered water-organic modifier system. The assumptions underlying the obtained results (no effects of pressure and temperature on the viscosity or retention coefficient) are critically reviewed, and can be inferred to only have a small effect on the general conclusions. It is also shown that, under the adopted assumptions, the kinetic plot theory also holds for operations where the flow rate varies with the time, as is the case for constant-pressure operation. Comparing both operation modes in a kinetic plot representing the maximal peak capacity versus time, it is theoretically predicted here that both modes can be expected to perform equally well in the fully C-term dominated regime (where $H$ varies linearly with the flow rate), while the constant pressure mode is advantageous for all lower flow rates. Near the optimal flow rate, and for linear gradients running from 5 to 95% organic modifier, time gains of the order of some 20% can be expected (or 25–30% when accounting for the fact that the constant pressure mode can be run without having to leave a pressure safety margin of 5–10% as is needed in the constant flow rate mode).



## 1. Introduction

Neglecting any possible adverse effects of viscous heating, a given chromatographic system will reach its kinetic optimum (defined as efficiency or peak capacity per unit of time) when it is operated at the maximal pressure ($\Delta P = \Delta P_{max}$). This has already been clearly demonstrated in the early days of chromatography [1,2] and also holds in isocratic as well as in gradient elution [3]. The latter has recently been demonstrated in a mathematically rigorous way and also allowed to extend the so-called kinetic plot theory [4–6] from isocratic to gradient elution operations [3]. The work on the gradient kinetic plot theory presented in [3] focused exclusively on constant flow rate (cF) operations, because this is the mode wherein all modern HPLC instruments are being operated. In this mode, the maximal pressure is however only reached during a brief instant, i.e. the instant at which the gradually varying mobile phase mixture that is being pumped through the column reaches its viscosity maximum. During the other moments of the run, the mobile phase is less viscous, so that the inlet pressure automatically drops. This suggests that a cF-gradient elution only makes a sub-optimal use of the available pressure during most of its run. As can be deduced from plots of the viscosity $\eta$ as a function of the fraction of organic modifier $\phi$ (see e.g. Refs. [7–10] or Fig. S-1 in the Supporting Material, SM), running a gradient from 5 to 95% methanol for example leads to an initial pressure that only makes up about 60% of the maximal pressure (which is reached when the composition in the column is about 50–50%), while the pressure at the end of the gradient even only amounts up to about 50% of the maximal pressure. For water-acetonitrile mixtures, these percentages respectively become 90% at the 5% composition and about 50% at the 95% composition.

As a consequence, it seems worthwhile to investigate whether gradient elution separations can be kinetically improved by leaving the constant flow mode and maintain the maximal pressure during

* Corresponding author. Tel.: +32 02 629 32 51; fax: +32 02 629 32 48.
*E-mail address:* gedesmet@vub.ac.be (G. Desmet).

0021-9673/$ – see front matter © 2010 Elsevier B.V. All rights reserved.
doi:10.1016/j.chroma.2010.12.086

**Nomenclature**

*Symbol list*

| | |
|---|---|
| $A$ | column cross section ($m^2$) |
| $C$ | concentration ($mol/m^3$) |
| cF | constant flow rate operation |
| cP | constant pressure operation |
| $D_{ax}$ | lumped axial dispersion coefficient ($m^2/s$) |
| $D_m$ | molecular diffusion coefficient ($m^3/s$) |
| $d_p$ | particle size (m) |
| $f_V$ | gradient program imposed at the column inlet as a function of $V'$ |
| $F$ | mobile phase flow rate ($m^3/s$) |
| $F_F$ | flow rate during a cF-mode run ($m^3/s$) |
| $F_{max}$ | maximum experimental flow rate ($m^3/s$) |
| $F_{P,av}$ | volume average flow rate in the cP-mode run ($m^3/s$) |
| $\Delta F_{av,\%}$ | relative increase in average flow rate of cP vs. cF mode |
| $H$ | (local) plate height (m) |
| $H_{eff}$ | column length averaged effective plate height (m) |
| ID | inner diameter (m) |
| $k$ | retention coefficient |
| $k_{loc}$ | local retention coefficient |
| $k_{loc,e}$ | local retention coefficient at point of elution |
| $K_{V0}$ | $u_0$-based column permeability ($m^2$) |
| KPL | kinetic performance limit |
| $L$ | column length (m) |
| $n_c$ | number of components in the sample |
| $n_p$ | peak capacity |
| $P_{F,av}$ | volume averaged inlet pressure in the cF-mode run (Pa) |
| $P_{F,max}$ | maximum column pressure experienced during a cF-run (Pa) |
| $\Delta P$ | column pressure drop (Pa) |
| $\Delta P_{max}$ | maximum allowed column or instrument pressure drop (Pa) |
| $\Delta P_{FP,av\%}$ | relative increase in average operating pressure of cP vs. cF mode |
| $t$ | time (s) |
| $t_G$ | gradient time (s) |
| $t_m$ | time spend by a component in the mobile phase (s) |
| $t_R$ | retention time (s) |
| $t_s$ | time spend by a component in an adsorbed state (s) |
| $t_V$ | volume-based reconstructed time, see Eq. (16) (s) |
| $t_0$ | column dead time (s) |
| $\Delta t_\%$ | relative reduction of the retention time of cP vs. cF mode in real time units |
| $T$ | temperature (K) |
| $u_R$ | retained species velocity (m/s) |
| $u_0$ | unretained species velocity (m/s) |
| $V$ | volume ($m^3$) |
| $V_G$ | gradient volume ($m^3$) |
| $V_m$ | volume of mobile phase passing through column when analytes are in the mobile phase ($m^3$) |
| $V_R$ | retention volume or the volume pumped through the column at the instant at which the peak centroid elutes from the column ($m^3$) |
| $V_s$ | volume of mobile phase passing through column when analytes are arrested in the stationary phase ($m^3$) |
| $V'$ | dimensionless volume, defined as $V' = V/V_0$ |
| $V_0$ | column dead volume, defined as $A\ \varepsilon_T\ L$ ($m^3$) |
| $x$ | axial position in the column (m) |
| $x'$ | dimensionless axial position in the column, defined as $x' = x/L$. |

*Greek symbols*

| | |
|---|---|
| $\varepsilon_T$ | total porosity |
| $\phi$ | fraction of organic modifier in mobile phase |
| $\phi_e$ | fraction of organic modifier in mobile phase at the end of the gradient |
| $\phi_0$ | fraction of organic modifier in mobile phase at start of the gradient |
| $\eta$ | viscosity (Pa s) |
| $\bar{\eta}$ | average column viscosity (Pa s) |
| $\lambda$ | column length rescaling factor, defined in Eq. (30) |
| $\nu$ | reduced mobile phase velocity, defined as $\nu = u_0\ d_p/D_m$ |
| $\pi$ | corrected pressure, defined as $\pi = K_{V0}\ \Delta P/L^2$ (Pa) |
| $\sigma_V$ | volumetric standard deviation ($m^3$) |

the whole gradient run, so as to operate the system at its kinetic optimum during the entire gradient run.

Contemplating on a comparison between this constant pressure mode (cP-mode) and the constant flow rate mode (cF-mode), the following key questions readily emerge:

(i) can the cP-mode and the cF-mode produce identical selectivities (i.e. can the cP-mode and the cF-mode lead to the same relative peak elution patterns)?
(ii) what is the decrease in analysis time that can be realized
(iii) how will the variable flow rate induced by the cP-mode affect the band broadening process
(iv) what is the overall difference in peak capacity and critical pair resolution that can be expected?
(v) is the length-extrapolation underlying the kinetic plot method [4–6] still valid?

Question (i) is raised because a general (i.e. sample-independent) comparison of the cF- and the cP-mode is only possible under the condition of an equal selectivity. Namely, if both modes would lead to a different separation selectivity, it would be possible to improve one mode with respect to the other by separately optimizing the gradient program used in the cP-mode and that used in the cF-mode. The outcome of this optimization would then depend on the retention behavior of the sample components, and the generality of the comparison would be lost.

In the present part I of our study, analytical as well as numerical calculations are presented that provide a theoretical answer to questions (i–v). In part II, the presented calculations are verified experimentally by performing a number of cF-mode and cP-mode operations.

Before proceeding, it is important to consider that, despite the fact that the gradient programs in any modern instrument are defined in time units, the analytes in fact follow the mobile phase gradient they experience in the volumetric units. This has been abundantly demonstrated by various authors, of which most of them started from the seminal work of Freiling [11] and Drake [12]. A good overview of the different contributions to the theory of gradient elution can be found in [13–15]. The prevalence of volume over time can for example be inferred from the fact that all early gradient elution expressions were established in volumetric units [16–19]. Physically, the necessity to work in volumetric coordinates can be understood by considering a gradient program as a succession of very short isocratic elution steps [11–13]. During each time step, the analytes are displaced isocratically over a volume $dV/(1+k)$, wherein $k$ is the retention factor corresponding to the elution strength $\phi$ prevailing during this step. Since the elution during this step is isocratic, the retention factor experienced

during the given elution step will be independent of the rate with which the given volume $dV$ is fed to the column. As a consequence, the distance over which the analytes will migrate during this step will only depend on the elution volume $dV$ and the mobile phase composition $\phi$, but not on the duration $dt$ of the step.

To simplify the notation and calculations, the calculations presented in the following sections (Sections 2–8) are made under the assumption of an isothermal operation and by assuming that the viscosity and the local retention factor are pressure-independent. The consequences of these assumptions are critically reviewed at the end of the paper in Section 9. Other simplifying assumptions were that the organic modifier is not-retained, that the peaks are narrow [20,21] and that the gradient dwell time and dwell volume is negligibly small.

## 2. Employed model and numerical solution method

To support and illustrate the presented analytical calculations, a numerical simulation study has been undertaken to model the effect of the operation mode on the separation performance. This has been done by solving the following time-dependent and one-dimensional axial dispersion model:

$$\frac{\partial C}{\partial t} = D_{ax,i} \cdot \frac{\partial^2 C}{\partial x^2} - u_R \cdot \frac{\partial C}{\partial x} \quad (\text{with } i = 1, n_c) \tag{1}$$

$$\frac{\partial \phi}{\partial t} = D_{ax,\phi} \cdot \frac{\partial^2 \phi}{\partial x^2} - u_0 \cdot \frac{\partial \phi}{\partial x} \tag{2}$$

Eq. (1) represents the mass balance of the analytes and is solved $n_c$ times ($n_c$ is the number of components in the sample) for each run, while Eq. (2) represents the mass balance of the mobile phase. Eq. (2) is solved using an inlet boundary condition wherein $\phi$ varies at the column inlet according to a given gradient elution program. Two types of gradient programs were considered: one wherein $\phi$ at $x = 0$ varies as a function of the elapsed time ($t$-based gradient) and one wherein $\phi$ at $x = 0$ varies as a function of the pumped volume ($V$-based gradient). For the cF-mode, the velocity $u_0$ was fixed. For the cP-mode, $u_0$ was calculated after each time step on the basis of the governing column-averaged viscosity using Darcy's law (see Eq. (5) further on) with a fixed inlet pressure, corresponding to the maximal pressure found during the cF-mode simulations. Because the $u_R$-velocity (with $u_R = u_0/(1 + k_{loc})$) considered in Eq. (1) depends on the local value of the retention coefficient, the simulations automatically incorporate the effect of peak compression [20–23]. The exact expressions employed for $D_{ax}$ (which depended on the local $k$ and $D_{mol}$-values as well as on the value of $u_0$), as well as the adopted numerical values for the different constants appearing in the model are given in SM, part 3.

The independent set of equations determined by Eqs. (1) and (2) was solved by applying the finite difference method to discretize the spatial derivatives (4th order for $\partial C/\partial x$; 3rd order for $\partial^2 C/\partial x^2$) and using a 4th-order Runge–Kutta algorithm to solve the resulting set of ordinary differential equations with respect to the time. The accuracy of this numerical method was demonstrated in previous work [3].

Practically relevant chromatographic conditions were chosen ($d_p = 2\,\mu m$, $\varepsilon_T = 0.7$, $T = 30\,^\circ C$, column ID 2.1 or 4.6 mm) and the mobile phase properties were based on experimentally measured values of water-methanol and water-acetonitrile mixtures [7]. As the numerical results were found to scale with the simulated column length in agreement with the theoretical expectations, most of the simulations (except those belonging to a series of control simulations conducted to investigate the effect of the column length, see e.g. Fig. S-6 in the SM) were run on a relatively short column (1.2 cm) to keep the simulation time ($t_{sim}$) within acceptable limits (i.e. between 2 and 5 days), since $t_{sim} \propto L^2$. The simulated column pressures ranged from the B-term regime of the van Deemter curve ($\Delta P = 10$ bar) to far into the C-term regime (600 bar).

The retention behavior of the test compounds was simulated by expressing that the logarithm of their local retention factor was a either a linear or a quadratic function of the local mobile phase composition. This allowed to demonstrate that the obtained results also hold under non-linear solvent strength conditions [18,21,23,24].

## 3. Relation between time and volume in gradient elution

### 3.1. General relationship between V and t

Assuming the non-compressibility of the liquid, the relation between the pumped volume and the elapsed time can generally be written as:

$$\frac{dV}{dt} = F(t) \tag{3}$$

#### 3.1.1. Constant F-mode

In the cF-mode, the flow rate is a constant ($F(t) = F_F$) so that Eq. (3) readily integrates into:

$$V = F_F \cdot t \tag{4}$$

#### 3.1.2. Constant P-mode

In the cP-mode on the other hand, the flow rate will inevitably vary with the time during a gradient elution, because of the varying average column viscosity $\bar{\eta}(t)$ appearing in Darcy's law ($\Delta P_{col}$ is a given constant in the cP-mode):

$$\frac{F(t)}{A \cdot \varepsilon_T} = u_0(t) = \frac{K_{V0} \cdot \Delta P_{col}}{\bar{\eta}(t) \cdot L} \tag{5}$$

In Eq. (5), $\bar{\eta}(t)$ is the column-length averaged viscosity of the mobile phase occupying the column at time $t$:

$$\bar{\eta}(t) = \int_0^1 \eta(x', t) \cdot dx' \tag{6}$$

As is described in detail in SM (Section 1.1), by writing $\bar{\eta}(t)$ in terms of run volume and by introducing a dimensionless volume $V'$ ($V' = V/V_0$, with $V_0 = A\,\varepsilon_T\,L$) and a dimensionless position in the column $x'$ ($x' = x/L$), Eq. (6) can be directly expressed in terms of the imposed volumetric gradient program $f_V$ as:

$$\bar{\eta}(V') = \int_0^1 \eta(f_V(V' - x')) \cdot dx' \tag{7}$$

Integrating Eq. (3) with the aid of Eqs. (5) and (6), and introducing a corrected pressure $\pi$ ($\pi = K_{V0}\,\Delta P/L^2$), it is found that:

$$t = \frac{1}{\pi} \cdot \int_0^{V'} \bar{\eta}(V') \cdot dV' \tag{8}$$

The general relation between time and the pumped volume in the cP-mode is now given by the combination of Eqs. (7) and (8), readily showing that, under the adopted assumptions, the relation between $V$ and $t$ in the constant cP-mode only depends on the applied (volume-based) gradient program $f_V$ and on the relation between the mobile phase viscosity and its composition $\phi$. The explicit solution of the combination of Eqs. (7) and (8) is discussed in Section 5.

### 3.2. Equivalence between time-based and volume-based gradient programs

As already mentioned in Section 1, the selective migration of the analytes under gradient conditions is exclusively determined

by how the mobile phase composition $\phi$ varies with the run volume. Despite this fact, mobile phase gradients are customarily programmed in time and not in volume. This is due to the fact that all modern instruments operate in the cF-mode, for which it makes no difference whether the gradient is programmed in time or volume, because both are in this case anyhow linearly related via Eq. (4).

In the cP-mode, this parallelism no longer holds. Given the prevalence of volume over time, this implies that gradient programs that are run in the cP-mode should be directly established in volumetric units. The latter however poses no fundamental challenge. Provided the pumped gradient volume can be continuously metered, changing $\phi$ as a function of the pumped volume is not fundamentally different from changing it as a function of elapsed time. Also, programming a volume-based gradient such that it produces the same selectivity as a given time-based gradient program in the cF-mode is quite straightforward due to the linear relationship that exists between $V$ and $t$ in the cF-mode. Using Eq. (4), even the most complex time-based gradient program established for use in the cF-mode can readily be transformed into an equivalent volume-based gradient program by transforming the characteristic times $t_i$ appearing in the original time-based program (with $t_i = t_a$, $t_b$, $t_c$, etc.) into the corresponding characteristic volumes $V_i$ needed in the volume-based program ($V_i = V_a$, $V_b$, $V_c$, etc.) using:

$$V_i = F_F \cdot t_i \tag{9}$$

To illustrate this, Table 1 shows how a relatively complex time-based gradient program, involving a non-linear part (see the gradient trace added to Fig. 1), can be directly turned into an equivalent volume-based program. The actual equivalence between both programs is further discussed in Section 4.

### 3.3. Time- versus volume-based chromatograms

Although it was certainly not unusual to see chromatograms that were plotted as a function of the eluted volume in the early years of chromatography [16], nearly all chromatograms are nowadays plotted in time units. This preference for time units originates from the early stages of automation of HPLC, wherein the generation of a constant flow and a constant paper feed was found to be easier than providing precise real-time value for passed eluent volume and referencing a detector signal to it.

Nevertheless, it should be kept in mind that time-based chromatograms only provide a truthful representation of the separation state in the column when the separation is run in the cF-mode. When the flow rate is not a constant, as is the case in the cP-mode, the time-based chromatogram can be misleading. This can for example be understood from the following thought-experiment. Consider an isocratic separation run at a constant flow rate and that the different compounds of the sample elute from the column at regular time intervals. Also assume that the band broadening is independent of the flow rate. If one would subsequently repeat the same separation but double the flow rate halfway the separation, while still recording the chromatogram in the time-based mode, it can be expected that the absolute distance between the peaks in the second part of the corresponding chromatogram will only be half of that in the first part of the chromatogram because the peaks would elute at double speed while the mutual selectivity between the different components is retained (the flow rate has no effect on the retention factor or the selectivity in the isocratic mode). The smaller distance between the peaks would however suggest that the selectivity of the column in the second part of the separation would be smaller than in the first part. This is however in conflict with the well-established fact that a change in flow rate cannot change the selectivity in an isocratic run so that one can only conclude that the time-based chromatogram is indeed misleading. Plotting the same accelerated separation in volumetric coordinates, the peaks in the first and the second part of the chromatogram would still be equally spaced because the double flow rate indeed halves the elution time but not the elution volume.

Time-based chromatograms can also be misleading in terms of peak width. In the column, the peaks have a certain spatial width, characterized by a spatial- or volume-based variance. In case of a variable flow rate, this volume-based variance can only be truthfully measured (apart from a $(1+k_e)$-factor [25]) if the detector signal is read-out in volumetric units. In time units, the double flow rate in the second part of the separation in the thought-experiment would lead to peaks that would appear only half as wide as they are in the separation where the flow rate was not accelerated halfway.

The misleading effect occurring when a time-axis chromatogram would be used under cP-conditions is illustrated in Fig. 1, where first a cF-mode separation is considered (running the complex gradient program shown in Table 1). In this mode (see Fig. 1a and b), volume and time are linearly related so that the time- and the volume-based chromatograms look identical provided the same relative scale for $V$ and $t$ is used. Considering the corresponding cP-mode separation on the other hand, time and volume are no longer linearly related so that the time- and volume-based chromatogram no longer display the same relative elution pattern (cf. Fig. 1c and d). The difference in apparent selectivity between the time- and volume-based chromatogram types is largest for the two last eluting components. This is due to the fact that the represented example relates to a case wherein the relation between $t$ and $V$ deviates most strongly from linearity at the end of the separation (see Fig. S-2 of the SM). The latter can also be noted from the fact that, compared to the first linear part, the second linear part of the gradient is in time units much steeper in the cP-mode (Fig. 1c) than in the cF-mode (Fig. 1a).

## 4. Effect of the operation mode on the elution pattern (separation selectivity)

The relative elution pattern mentioned in the discussion of Fig. 1 here above is customarily quantified by the retention factors of the different analytes. Depending on the selected $x$-axis of the chromatogram (time- or volume-based), either a volume-based (Section 4.1) or a time-based retention factor (Section 4.2) will be obtained. Although it has been shown in Section 3.3 that only the volume-based chromatograms provide a correct representation of the actual separation selectivity inside the column, we also provide the equations for the retention times and factors that will be observed in the real time- chromatogram as these expressions can be used to calculate the gain in analysis time that can be obtained by switching from the cF- to the cP-mode.

### 4.1. Selectivity in the volume-based chromatograms

In a volume-based chromatogram, the retention factor of a given analyte is defined as:

$$k_{eff,V} = \frac{V_R - V_0}{V_0} = V'_R - 1 \tag{10}$$

wherein $V_R$ is the volume pumped through the column at the instant at which the center of mass (peak centroid) elutes from the column.

Adopting the classical treatment of Snyder [16,18] and Jandera [14,19], the value of $k_{eff,V}$ can be readily calculated by expressing that, at the moment at which the peak centroid has been displaced over a volume $dV_m$ in the mobile phase, a given volume $dV_s$ will have passed "unnoticed" through the peak centroid, i.e. without having generated any additional displacement of the peak. As such, the volume $dV_s$ corresponds to the volume passing through the

**Table 1**
Example of the equivalence between a gradient program written in time coordinates (a) and in volumetric coordinates (b).

| | | |
|---|---|---|
| **(a) Time-based gradient program** | | |
| $f(t)=\phi_0$ | for $t<t_a$ | (T-1) |
| $f(t)=\phi_0+a\cdot(t-t_a)$ | for $t_a<t<t_b$ with $a=\frac{\phi_b-\phi_0}{t_b-t_a}$ | (T-2) |
| $f(t)=\phi_0+a\cdot(t_b-t_a)+b\cdot(t-t_b)$ | for $t_b<t<t_c$ with $b=\left(\frac{\phi_c-\phi_b}{t_c-t_b}\right)^n$ | (T-3) |
| $f(t)=\phi_0+a\cdot(t_b-t_a)+b\cdot(t_c-t_b)^n+c\cdot(t-t_c)$ | for $t_b<t<t_c$ with $c=\frac{\phi_{\mathrm{end}}-\phi_c}{t_{\mathrm{end}}-t_c}$ | (T-4) |
| and with: $\phi_b=\phi_0+a\cdot(t_b-t_a)$; $\phi_c=\phi_0+a\cdot(t_b-t_a)+b\cdot(t_c-t_b)^n$ | | (T-5) |
| **(b) Volume-based gradient program** | | |
| $f(V)=\phi_0$ | for $V<V_a$ | (T-6) |
| $f(t)=\phi_0+a\cdot(V-V_a)$ | for $V_a<V<V_b$ with $a=\frac{\phi_b-\phi_0}{V_b-V_a}$ | (T-7) |
| $f(t)=\phi_0+a\cdot(V_b-V_a)+b\cdot(V-V_b)$ | for $V_b<V<V_c$ with $b=\left(\frac{\phi_c-\phi_b}{V_c-V_b}\right)^n$ | (T-8) |
| $f(V)=\phi_0+a\cdot(V_b-V_a)+b\cdot(V_c-V_b)^n+c\cdot(V-V_c)$ | for $V_b<V<V_c$ with $c=\frac{\phi_{end}-\phi_c}{V_{end}-V_c}$ | (T-9) |
| and with: $\phi_b=\phi_0+a\cdot(V_b-V_a)$; $\phi_c=\phi_0+a\cdot(V_b-V_a)+b\cdot(V_c-V_b)^n$ | | (T-10) |

column during the instants at which the analytes are arrested in the stationary phase. By definition, the sum of both volumes is equal to the total pumped volume $dV$ during the considered interval:

$$dV = dV_m + dV_s \tag{11}$$

while the ratio between both volumes is given by $k_{loc}$, the local retention coefficient:

$$dV_m = \frac{dV_s}{k_{loc}} \tag{12}$$

As elaborated in Section 1, the analytes migrating through a column in general obey a gradient program as a function of the pumped volume and not as a function of the elapsed time. It should hence be noted that Eq. (12) is a more fundamental definition of the local retention factor than the more customary employed time-based definition ($dt_m = dt_s/k_{loc}$ [15,21,23,24]), which is only valid when time and volume are linearly related, i.e. in the cF-mode.

By integrating Eq. (12) over the gradient volume $V_R$, it can be shown (see Section 1.2 in the SM) that the volume-based retention coefficient of any given analyte will be fully determined by the volume-based gradient program $f_V$. Since the derivation does not require the assumption of a constant flow rate (see SM), this holds for constant as well as for variable flow rate operations. This implies that the cF- and the cP-mode can be expected to yield the same

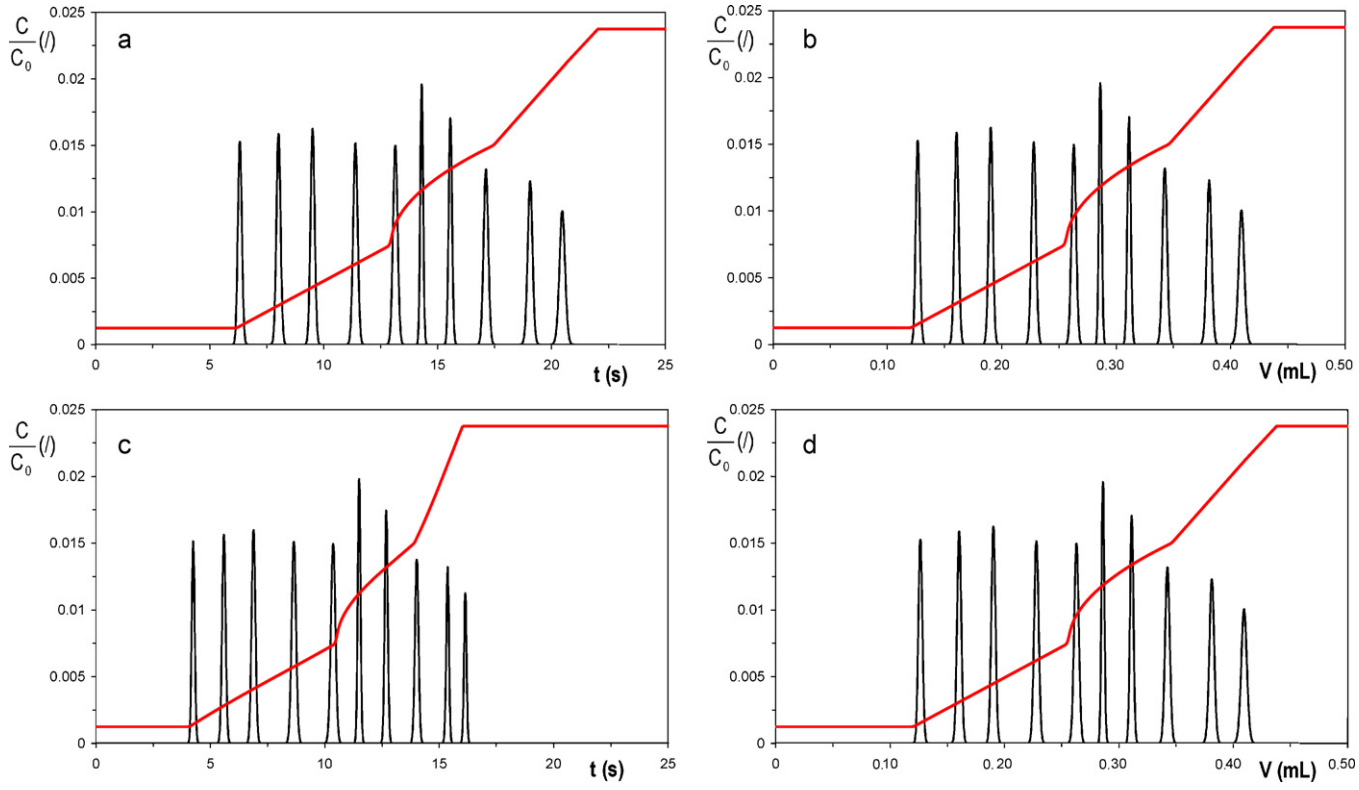


**Fig. 1.** Example of simulated chromatograms demonstrating equivalence between the cF- and the cP-mode when applying the same volume-based gradient program: (a) cF-mode, time-chromatogram, (b) cF-mode, volume-chromatogram, (c) cP-mode, time-chromatogram, (d) cP-mode, volume-chromatogram. Applied gradient profile represented by the red line (see also Eqs. (T1)–(T10) in Table 1). Column length = 1.2 cm and ID = 4.6 mm, $V_0$ = 0.03 mL, cF-mode flow rate = 1.2 mL/min with a methanol–water gradient running between 10 and 90%. (For interpretation of the references to color in text, the reader is referred to the web version of the article.)

$k_{eff,V}$-value provided the same volume-based gradient program is run in both modes. This is illustrated in Fig. 1.

The above calculation parallels the recent work presented by Nikitas and Pappa-Louisi investigating the problem of retention time prediction of mobile phase gradient elution under variable flow rate [13,26–28].

### 4.2. Selectivity in the time-based chromatogram

In a time-based chromatogram, the effective retention factor is generally defined as:

$$k_{eff,t} = \frac{t_R - t_0}{t_0} \tag{13}$$

Knowing from the above section that the volume $V_R$ needed to elute a given component from the column is independent of the operation mode, we can put $V = V_R$ in resp. Eqs. (4) and (8) to compare the expected elution time in the cF-mode (cf. Eq. (3)):

$$t_R = \frac{V_R}{F_F} \tag{14a}$$

with that in the cP-mode:

$$t_R = \frac{1}{\pi} \int_0^{V'_R} \bar{\eta}(f_V(V')) \cdot dV' \tag{14b}$$

Both expressions only return the same $t_R$ provided $\bar{\eta}$ remains constant, as is the case in an isocratic run. Since $\bar{\eta}$ will generally vary with the pumped volume during a gradient separation, Eqs. (14a) and (14b) will generally lead to different $t_R$-values.

The two operation modes in general also lead to a different breakthrough time for an unretained component ($t_0$-time marker). In the cF-mode, this component will elute after a time $t_0$, given by:

$$t_0 = \frac{V_0}{F_F} \tag{15a}$$

whereas an unretained component will elute at a time determined by Eq. (7) in the cP-mode:

$$t_0^* = \frac{1}{\pi} \int_0^1 \bar{\eta}(V') \cdot dV' \tag{15b}$$

Again both values will generally differ when $\bar{\eta}$ varies during the course of the separation. To prevent any misunderstanding with the generally adopted definition of $t_0$ (Eq. (15a)), an asterisk has been added to the $t_0$-symbol used in Eq. (15b).

## 5. Relation between time-based and volume-based chromatograms and introduction of reconstructed time axis

The previous sections have emphasized the importance of switching from time to volumetric units to establish gradient programs and record chromatograms in cases where the flow rate varies with the time, as is the case in the presently investigated cP-mode.

Although there are no fundamental limitations to make this switch, it might be uncomfortable to analysts who are accustomed to thinking and reasoning in time units. To circumvent this possible "mental" objection, the volumetric units can, if desired, readily be turned into a volume based reconstructed time $t_V$ by dividing the original volume data by the flow rate $F_F$ used in the cF-mode separation one is comparing with:

$$t_V = \frac{V}{F_F} \tag{16}$$

As the reconstructed time $t_V$ is based on a simple linear transformation of the volume-coordinate, programming gradients and recording chromatograms in reconstructed time units is fully equivalent to using volumetric units. This is illustrated in Fig. 2, showing the transition between a representation of the gradient program and its corresponding separation in the volume-based mode to a representation versus the reconstructed time axis. As can be noted, both chromatograms display exactly the same selectivity (relative position of the peaks).

Using reconstructed time units has the additional advantage that it yields chromatograms with identical elution times as in the time-based chromatogram obtained in the cF-mode, as can be witnessed from the exact agreement between Fig. 2b with Fig. 1a. Hence, when comparing a cF- and a cP-mode gradient separation that runs the same volume-based gradient program, the cP-mode will, in reconstructed time coordinates, produce exactly the same elution pattern as the real time chromatogram in the cF-mode. In real time units however, the cP-mode produces the given selectivity in a shorter time. This is illustrated in Fig. 1, where the cP-mode separation only lasts some 17 s in real time units (Fig. 1c) whereas the same selectivity is only obtained after some 21 s in the cF-mode (Fig. 1a).

The reconstructed time axis chromatogram (Fig. 2b) that can be established for the cP-mode separation also directly displays the correct component selectivity (something which does not hold for the real time chromatogram). This can be inferred from the fact that the retention factors that would be read out for the different eluting compounds in the virtual time chromatogram would all be equal to the corresponding volume-based retention factors (which represent the only correct selectivity) via:

$$k_{eff,\text{virtual time}} = \frac{t_{V,R}}{t_{V,0}} - 1 = \frac{t_{V,R} \cdot F_F}{t_{V,0} \cdot F_F} - 1 = \frac{V_R}{V_0} - 1 = k_{eff,V} \tag{17}$$

which is directly based on the use of the reconstructed time definition given by Eq. (16).

## 6. Potential gain in analysis time when switching from the cF- to the cP-mode

To exactly calculate how much faster the cP-mode can produce a given selectivity than the cF-mode, the retention time of the last eluting compound predicted by Eq. (14a) should be compared to that predicted by Eq. (14b). Since the last compound will in both modes elute with the same $k_{eff,V}$(last), this calculation should be made by putting $V'_R = k_{eff,V}(\text{last}) + 1$ in both Eqs. (14a) and (14b). A speed comparison based on the last eluting compound of a given sample is however not very general, as the outcome might depend on the elution properties of the compound. It has therefore been preferred to compare the retention time of a component that would elute simultaneously with the end of a linear gradient (in which case we assume the separation ends when the end of the gradient breaks through at the column end). In this case, Eqs. (14a) and (14b) have to be calculated with $V'_R = V'_G + 1$, wherein $V'_G$ is the relative gradient volume equal to $V_G/V_0$. If preferred, $V'_G$ can also be expressed in time units, so that $V'_R = t_G F_F/V_0 + 1$, wherein $t_G$ is the time corresponding to the end of the gradient program in the cF-mode

For the cP-mode, Eq. (14b) with $V'_R = V'_G + 1$ leads to:

$$t_R = \frac{1}{\pi} \cdot \int_0^{V'_G+1} \left[ \int_0^1 \eta(\phi(0, V' - x')) \cdot dx' \right] \cdot dV' \tag{18}$$

with

$$\phi(0, V' - x') = f_V(0) = \phi_0 \qquad -1 \le V' - x' \le 0 \tag{19a}$$

$$\phi(0, V' - x') = f_V(V' - x') \qquad 0 \le V' - x' \le V'_G \tag{19b}$$

$$\phi(0, V' - x') = f_V(V'_G) = \phi_e \qquad V'_G \le V' - x' \le V'_G + 1 \tag{19c}$$

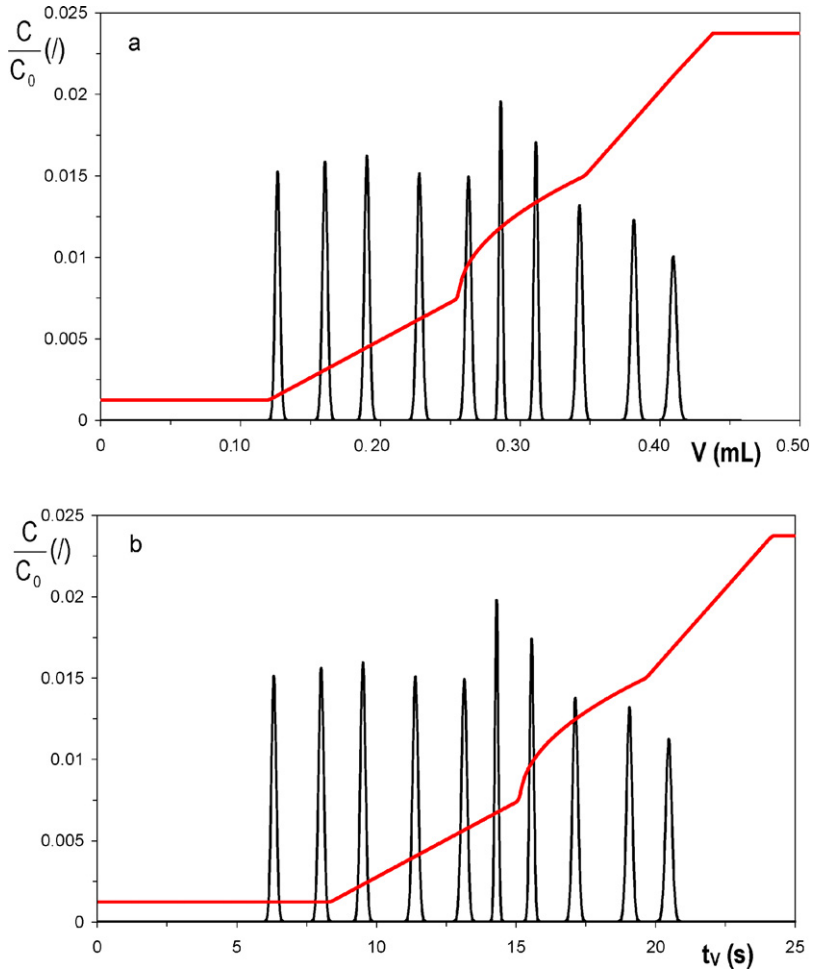


**Fig. 2.** Identical elution pattern obtained when plotting a cP-mode separation in (a) volumetric coordinates and in (b) reconstructed time axis coordinates (using $t_V = V/F_F$). Same separation conditions as in Fig. 1.

wherein Eq. (19a) expresses that the column is filled with a mobile phase with composition $\phi_0$ at the start of the separation, and that this volume is gradually flushed out during the period wherein $V' \leq 1$. Eq. (19c) expresses that once the gradient program is finished at the inlet, it still takes the elution of one additional void volume (corresponding to one unity of the reduced volume $V'$) before the end of the gradient reaches the end of the column.

For the cF-mode, $\eta = \eta_{max}$ = constant, so that the integral in Eq. (18) can simply be replaced by:

$$t_R = \frac{1}{\pi} \cdot \eta_{max} \cdot (V'_G + 1) \tag{20}$$

Defining the gain in analysis time $\Delta t_{\%}$ as the relative reduction of the retention time in both modes (and calculated in real time units), it should first be noted that this gain is also equal to the average increase in flow rate $\Delta F_{av,\%}$ that can be realized when switching to the cP-mode. Directly applying Darcy's law, this relative gain is in fact also equal to the relative increase in pressure $\Delta P_{FP,av\%}$ that can be realized when going from the cF- to the cP-mode, so that:

$$\Delta t_{\%} = \frac{(t_{R,cF-mode} - t_{R,cP-mode})}{t_{R,cF-mode}} = \frac{(F_{P,av} - F_F)}{F_F} = \Delta F_{FP,av\%} = \frac{(P_{F,max} - P_{F,av})}{P_{F,max}} = \Delta P_{FP,av\%} \tag{21}$$

wherein $P_{F,av}$ is the volume averaged inlet pressure in the cF-mode run, $F_{P,av}$ is the average flow rate in the cP-mode run and wherein $P_{F,max}$ is the maximum pressure experienced during a cF-run (see resp. Fig. 4a and c further on for a graphical illustration of $P_{F,av}$, $F_{P,av}$ and $P_{F,max}$).

Subsequently filling in the cF-mode and the cP-mode analysis time expression into Eq. (21) yields:

$$\Delta t_{\%} = \frac{\int_0^{V'_G+1} \left[ \int_0^1 \eta(\phi(0, V' - x')) \cdot dx' \right] \cdot dV'}{\eta_{max} \cdot (V'_G + 1)} - 1 \tag{22}$$

Tables 2–5 show the results produced by Eq. (22) for linear water–methanol (Tables 2 and 3) and water–acetonitrile gradients (Tables 4 and 5). For each mixture type, the whole space of possible start and end compositions is covered in steps of 5%. In addition, also two strongly different degrees of gradient steepness have been considered for each mixture type: a very steep gradient, with $V'_G = V_G/V_0 = 3$ (Tables 2 and 4) and a rather shallow gradient with $V'_G = V_G/V_0 = 15$ (Tables 3 and 5).

The tabulated data were calculated using the relation between the viscosity and the fraction organic modifier obtained in [7] for a pressure of 500 bars (intermediate pressure between column inlet and outlet for a separation run at 1000 bar) and a temperature of 30 °C. For methanol, two second order polynomial fittings were used (for the intervals $0 < \phi < 50$ and $50 < \phi < 100$ vol.% MeOH), whereas for acetonitrile, a second order and third order polynomial were used (for the intervals $0 < \phi < 20$ and $20 < \phi < 100$ vol.% ACN respectively). A fitting quality of $SSE < 0.5\%$ was obtained. The expression for the fits, as well as their graphical representation, is given in SM (see Fig. S-1). The SM also contains tables for other

**Table 2**
Numerical values of $\Delta t_{\%}$ (see Eq. (21)) for methanol–water gradients at an average pressure of 500 bar for a gradient steepness of $V_G/V_0 = 3$ (with $V'_R(\text{last}) = V'_G + 1$) for different values of the initial ($\phi_0$) and final ($\phi_e$) mobile phase composition.

| $\phi_0$ (%) | $\phi_e$ (%) | | | | | | | | | | | | | | | | | | |
|---|---|---|---|---|---|---|---|---|---|---|---|---|---|---|---|---|---|---|---|
| | 10 | 15 | 20 | 25 | 30 | 35 | 40 | 45 | 50 | 55 | 60 | 65 | 70 | 75 | 80 | 85 | 90 | 95 | 100 |
| 5 | 5.21 | 8.97 | 11.72 | 13.72 | 15.16 | 16.14 | 16.74 | 17.01 | 16.97 | 15.48 | 14.26 | 13.87 | 13.96 | 14.50 | 15.49 | 16.94 | 18.85 | 21.23 | 24.08 |
| 10 | | 4.32 | 7.51 | 9.87 | 11.59 | 12.81 | 13.60 | 14.03 | 14.12 | 12.73 | 11.69 | 11.44 | 11.65 | 12.32 | 13.44 | 15.02 | 17.06 | 19.57 | 22.56 |
| 15 | | | 3.60 | 6.29 | 8.29 | 9.73 | 10.71 | 11.30 | 11.52 | 10.23 | 9.39 | 9.27 | 9.61 | 10.40 | 11.66 | 13.37 | 15.56 | 18.21 | 21.33 |
| 20 | | | | 3.00 | 5.25 | 6.91 | 8.07 | 8.81 | 9.16 | 7.97 | 7.35 | 7.35 | 7.82 | 8.75 | 10.15 | 12.01 | 14.34 | 17.13 | 20.39 |
| 25 | | | | | 2.49 | 4.35 | 5.68 | 6.56 | 7.03 | 5.97 | 5.55 | 5.69 | 6.30 | 7.38 | 8.93 | 10.94 | 13.41 | 16.36 | 19.77 |
| 30 | | | | | | 2.04 | 3.53 | 4.55 | 5.15 | 4.23 | 4.00 | 4.29 | 5.06 | 6.29 | 8.00 | 10.16 | 12.79 | 15.89 | 19.46 |
| 35 | | | | | | | 1.64 | 2.79 | 3.50 | 2.77 | 2.72 | 3.17 | 4.11 | 5.51 | 7.38 | 9.71 | 12.50 | 15.76 | 19.49 |
| 40 | | | | | | | | 1.27 | 2.09 | 1.58 | 1.71 | 2.36 | 3.47 | 5.05 | 7.10 | 9.60 | 12.56 | 15.99 | 19.88 |
| 45 | | | | | | | | | 0.92 | 0.67 | 1.04 | 1.89 | 3.21 | 4.97 | 7.19 | 9.87 | 13.01 | 16.64 | 20.75 |
| 50 | | | | | | | | | | 0.22 | 0.90 | 2.03 | 3.62 | 5.66 | 8.14 | 11.09 | 14.48 | 18.33 | 22.63 |
| 55 | | | | | | | | | | | 0.83 | 2.12 | 3.87 | 6.07 | 8.73 | 11.84 | 15.40 | 19.43 | 23.90 |
| 60 | | | | | | | | | | | | 1.47 | 3.40 | 5.80 | 8.66 | 11.98 | 15.77 | 20.02 | 24.73 |
| 65 | | | | | | | | | | | | | 2.15 | 4.78 | 7.89 | 11.48 | 15.55 | 20.10 | 25.12 |
| 70 | | | | | | | | | | | | | | 2.92 | 6.34 | 10.27 | 14.69 | 19.62 | 25.05 |
| 75 | | | | | | | | | | | | | | | 3.82 | 8.17 | 13.06 | 18.48 | 24.43 |
| 80 | | | | | | | | | | | | | | | | 4.91 | 10.41 | 16.48 | 23.13 |
| 85 | | | | | | | | | | | | | | | | | 6.32 | 13.28 | 20.88 |
| 90 | | | | | | | | | | | | | | | | | | 8.23 | 17.20 |

**Table 3**
Numerical values of $\Delta t_{\%}$ (see Eq. (21)) for methanol–water gradients at an average pressure of 500 bar for a gradient steepness of $V_G/V_0 = 15$ (with $V'_R(\text{last}) = V'_G + 1$) for different values of the initial ($\phi_0$) and final ($\phi_e$) mobile phase composition.

| $\phi_0$ (%) | $\phi_e$ (%) | | | | | | | | | | | | | | | | | | |
|---|---|---|---|---|---|---|---|---|---|---|---|---|---|---|---|---|---|---|---|
| | 10 | 15 | 20 | 25 | 30 | 35 | 40 | 45 | 50 | 55 | 60 | 65 | 70 | 75 | 80 | 85 | 90 | 95 | 100 |
| 5 | 5.20 | 8.92 | 11.61 | 13.54 | 14.88 | 15.76 | 16.23 | 16.36 | 16.16 | 14.65 | 13.60 | 12.95 | 12.72 | 12.89 | 13.48 | 14.48 | 15.90 | 17.73 | 19.97 |
| 10 | | 4.31 | 7.46 | 9.76 | 11.41 | 12.54 | 13.23 | 13.54 | 13.49 | 12.10 | 11.17 | 10.66 | 10.57 | 10.89 | 11.64 | 12.80 | 14.38 | 16.38 | 18.79 |
| 15 | | | 3.59 | 6.25 | 8.19 | 9.56 | 10.45 | 10.93 | 11.04 | 9.77 | 8.97 | 8.60 | 8.66 | 9.14 | 10.05 | 11.38 | 13.13 | 15.30 | 17.88 |
| 20 | | | | 2.99 | 5.21 | 6.81 | 7.90 | 8.55 | 8.80 | 7.65 | 6.99 | 6.77 | 6.99 | 7.65 | 8.72 | 10.23 | 12.15 | 14.50 | 17.26 |
| 25 | | | | | 2.48 | 4.30 | 5.58 | 6.40 | 6.79 | 5.77 | 5.25 | 5.19 | 5.59 | 6.41 | 7.67 | 9.35 | 11.46 | 13.99 | 16.94 |
| 30 | | | | | | 2.03 | 3.49 | 4.46 | 4.99 | 4.10 | 3.75 | 3.87 | 4.44 | 5.46 | 6.90 | 8.78 | 11.08 | 13.80 | 16.94 |
| 35 | | | | | | | 1.63 | 2.75 | 3.41 | 2.67 | 2.50 | 2.82 | 3.59 | 4.81 | 6.45 | 8.53 | 11.02 | 13.94 | 17.28 |
| 40 | | | | | | | | 1.26 | 2.05 | 1.49 | 1.54 | 2.08 | 3.07 | 4.49 | 6.35 | 8.63 | 11.33 | 14.45 | 17.99 |
| 45 | | | | | | | | | 0.91 | 0.60 | 0.92 | 1.70 | 2.93 | 4.58 | 6.65 | 9.14 | 12.04 | 15.37 | 19.11 |
| 50 | | | | | | | | | | 0.21 | 0.83 | 1.87 | 3.32 | 5.19 | 7.47 | 10.16 | 13.28 | 16.80 | 20.74 |
| 55 | | | | | | | | | | | 0.82 | 2.05 | 3.70 | 5.77 | 8.25 | 11.16 | 14.48 | 18.21 | 22.37 |
| 60 | | | | | | | | | | | | 1.45 | 3.32 | 5.62 | 8.35 | 11.50 | 15.07 | 19.07 | 23.50 |
| 65 | | | | | | | | | | | | | 2.13 | 4.71 | 7.72 | 11.17 | 15.06 | 19.38 | 24.15 |
| 70 | | | | | | | | | | | | | | 2.90 | 6.26 | 10.08 | 14.36 | 19.10 | 24.30 |
| 75 | | | | | | | | | | | | | | | 3.80 | 8.08 | 12.86 | 18.12 | 23.87 |
| 80 | | | | | | | | | | | | | | | | 4.89 | 10.31 | 16.26 | 22.74 |
| 85 | | | | | | | | | | | | | | | | | 6.29 | 13.17 | 20.64 |
| 90 | | | | | | | | | | | | | | | | | | 8.20 | 17.08 |

**Table 4**
Numerical values of $\Delta t_{\%}$ (see Eq. (21)) for acetonitrile–water gradients at an average pressure of 500 bar for a gradient steepness of $V_G/V_0 = 3$ (with $V'_R(\text{last}) = V'_G + 1$) for different values of the initial ($\phi_0$) and final ($\phi_e$) mobile phase composition.

| $\phi_0$ (%) | $\phi_e$ (%) | | | | | | | | | | | | | | | | | | |
|---|---|---|---|---|---|---|---|---|---|---|---|---|---|---|---|---|---|---|---|
| | 10 | 15 | 20 | 25 | 30 | 35 | 40 | 45 | 50 | 55 | 60 | 65 | 70 | 75 | 80 | 85 | 90 | 95 | 100 |
| 5 | 2.09 | 3.26 | 3.64 | 2.96 | 2.74 | 2.87 | 3.28 | 3.95 | 4.85 | 5.95 | 7.22 | 8.65 | 10.22 | 11.89 | 13.66 | 15.49 | 17.36 | 19.26 | 21.16 |
| 10 | | 1.39 | 1.95 | 1.50 | 1.47 | 1.76 | 2.32 | 3.13 | 4.16 | 5.37 | 6.76 | 8.29 | 9.95 | 11.71 | 13.55 | 15.46 | 17.40 | 19.37 | 21.33 |
| 15 | | | 0.74 | 0.52 | 0.68 | 1.13 | 1.84 | 2.78 | 3.92 | 5.24 | 6.72 | 8.35 | 10.11 | 11.98 | 13.96 | 16.00 | 18.08 | 20.19 | 22.29 |
| 20 | | | | 0.08 | 0.42 | 1.05 | 1.92 | 3.02 | 4.32 | 5.81 | 7.45 | 9.24 | 11.15 | 13.15 | 15.22 | 17.35 | 19.51 | 21.68 | 23.83 |
| 25 | | | | | 0.45 | 1.17 | 2.13 | 3.31 | 4.70 | 6.26 | 7.99 | 9.84 | 11.81 | 13.88 | 16.01 | 18.19 | 20.40 | 22.61 | 24.80 |
| 30 | | | | | | 0.81 | 1.87 | 3.14 | 4.62 | 6.27 | 8.07 | 10.01 | 12.06 | 14.20 | 16.40 | 18.64 | 20.91 | 23.18 | 25.43 |
| 35 | | | | | | | 1.15 | 2.53 | 4.10 | 5.85 | 7.75 | 9.78 | 11.91 | 14.14 | 16.42 | 18.75 | 21.09 | 23.43 | 25.74 |
| 40 | | | | | | | | 1.48 | 3.16 | 5.01 | 7.02 | 9.15 | 11.39 | 13.72 | 16.10 | 18.52 | 20.95 | 23.38 | 25.77 |
| 45 | | | | | | | | | 1.80 | 3.77 | 5.89 | 8.15 | 10.51 | 12.94 | 15.44 | 17.97 | 20.51 | 23.03 | 25.52 |
| 50 | | | | | | | | | | 2.11 | 4.37 | 6.75 | 9.25 | 11.82 | 14.44 | 17.09 | 19.75 | 22.39 | 24.99 |
| 55 | | | | | | | | | | | 2.41 | 4.95 | 7.59 | 10.32 | 13.09 | 15.89 | 18.68 | 21.46 | 24.18 |
| 60 | | | | | | | | | | | | 2.71 | 5.53 | 8.42 | 11.36 | 14.33 | 17.28 | 20.21 | 23.08 |
| 65 | | | | | | | | | | | | | 3.01 | 6.10 | 9.23 | 12.39 | 15.53 | 18.63 | 21.66 |
| 70 | | | | | | | | | | | | | | 3.31 | 6.66 | 10.03 | 13.38 | 16.68 | 19.90 |
| 75 | | | | | | | | | | | | | | | 3.60 | 7.22 | 10.80 | 14.33 | 17.77 |
| 80 | | | | | | | | | | | | | | | | 3.89 | 7.75 | 11.54 | 15.23 |
| 85 | | | | | | | | | | | | | | | | | 4.17 | 8.25 | 12.22 |
| 90 | | | | | | | | | | | | | | | | | | 4.42 | 8.70 |

**Table 5**
Numerical values of $\Delta t_{\%}$ (see Eq. (21)) for acetonitrile–water gradients at an average pressure of 500 bar for a gradient steepness of $V_G/V_0 = 15$ (with $V'_R(\text{last}) = V'_G + 1$) for different values of the initial ($\phi o$) and final ($\phi_e$) mobile phase composition.

| $\phi_0$ (%) | $\phi_e$ (%) | | | | | | | | | | | | | | | | | | |
|---|---|---|---|---|---|---|---|---|---|---|---|---|---|---|---|---|---|---|---|
| | 10 | 15 | 20 | 25 | 30 | 35 | 40 | 45 | 50 | 55 | 60 | 65 | 70 | 75 | 80 | 85 | 90 | 95 | 100 |
| 5 | 2.07 | 3.18 | 3.46 | 2.70 | 2.37 | 2.40 | 2.71 | 3.29 | 4.10 | 5.12 | 6.32 | 7.68 | 9.19 | 10.81 | 12.55 | 14.36 | 16.24 | 18.17 | 20.13 |
| 10 | | 1.37 | 1.88 | 1.34 | 1.23 | 1.45 | 1.95 | 2.69 | 3.65 | 4.80 | 6.13 | 7.61 | 9.22 | 10.95 | 12.78 | 14.69 | 16.65 | 18.65 | 20.68 |
| 15 | | | 0.72 | 0.43 | 0.55 | 0.96 | 1.63 | 2.52 | 3.61 | 4.89 | 6.33 | 7.92 | 9.63 | 11.45 | 13.36 | 15.35 | 17.38 | 19.45 | 21.54 |
| 20 | | | | 0.07 | 0.39 | 0.96 | 1.76 | 2.77 | 3.98 | 5.36 | 6.91 | 8.59 | 10.39 | 12.30 | 14.29 | 16.34 | 18.45 | 20.58 | 22.72 |
| 25 | | | | | 0.44 | 1.12 | 2.04 | 3.16 | 4.47 | 5.95 | 7.59 | 9.36 | 11.24 | 13.22 | 15.28 | 17.41 | 19.57 | 21.75 | 23.94 |
| 30 | | | | | | 0.80 | 1.83 | 3.06 | 4.48 | 6.06 | 7.80 | 9.66 | 11.64 | 13.71 | 15.85 | 18.05 | 20.28 | 22.53 | 24.78 |
| 35 | | | | | | | 1.14 | 2.49 | 4.03 | 5.72 | 7.56 | 9.53 | 11.61 | 13.78 | 16.01 | 18.30 | 20.62 | 22.95 | 25.27 |
| 40 | | | | | | | | 1.47 | 3.13 | 4.95 | 6.91 | 9.00 | 11.19 | 13.46 | 15.81 | 18.19 | 20.61 | 23.03 | 25.44 |
| 45 | | | | | | | | | 1.79 | 3.74 | 5.84 | 8.06 | 10.37 | 12.78 | 15.24 | 17.74 | 20.27 | 22.79 | 25.30 |
| 50 | | | | | | | | | | 2.10 | 4.34 | 6.71 | 9.17 | 11.71 | 14.31 | 16.94 | 19.60 | 22.24 | 24.87 |
| 55 | | | | | | | | | | | 2.41 | 4.93 | 7.56 | 10.26 | 13.01 | 15.80 | 18.59 | 21.38 | 24.13 |
| 60 | | | | | | | | | | | | 2.71 | 5.51 | 8.39 | 11.32 | 14.28 | 17.24 | 20.18 | 23.08 |
| 65 | | | | | | | | | | | | | 3.01 | 6.09 | 9.22 | 12.37 | 15.51 | 18.63 | 21.70 |
| 70 | | | | | | | | | | | | | | 3.31 | 6.66 | 10.03 | 13.38 | 16.70 | 19.96 |
| 75 | | | | | | | | | | | | | | | 3.61 | 7.22 | 10.81 | 14.36 | 17.83 |
| 80 | | | | | | | | | | | | | | | | 3.89 | 7.76 | 11.57 | 15.28 |
| 85 | | | | | | | | | | | | | | | | | 4.17 | 8.27 | 12.26 |
| 90 | | | | | | | | | | | | | | | | | | 4.43 | 8.73 |

average column pressures (e.g. for 300 bar and 50 bar, corresponding to a column operating pressure of respectively 600 and 100 bar) and for gradients where the last component elutes at $V'_R = V'_G$ and not at $V'_R = V'_G + 1$ (=moment of elution of end of gradient) as is the case in Tables 2–5. If desired, a simplified version of the integral given in Eq. (22) can be approximated using a discrete sum approach wherein the gradient is divided in short segments (as e.g. described in [13,26–28]).

A first general observation that can be made from Tables 2–5 is that the relative gain is only weakly affected by the gradient steepness, as the values for the same $\phi_0$- and $\phi_e$-case only vary relatively weakly between the steep gradient case and the weak gradient case (compare corresponding data entries in Tables 2 and 3 for water-methanol gradients and compare between Tables 4 and 5 for water-acetonitrile gradients). The gain for methanol gradients is always larger for the fastest gradient, with a maximum absolute difference in $\Delta t_{\%}$ of 4.1% for a gradient running from 5 to 100% between the two presented steepnesses. For acetonitrile gradients, the largest difference in $\Delta t_{\%}$ in only 1.1% and in some cases the gain is even slightly larger in case of the more shallow gradient. For the cases with $V'_R = V'_G$, the behavior is more complex as can be seen from Tables S-3, S-4, S-6 and S-7 in the SM, part 4.

The most important observation that can be made from Tables 2–5 is the order of magnitude of the gain in analysis time that can be expected when switching to the cP-mode. For the case of a typical scouting gradient running between 5 and 95% of organic modifier, the entries for the 5–95%-case in Tables 2–5 show that this gain will be very similar for the ACN- and the MeOH-case and can be expected to lie around 19.5% for methanol-based gradients and around 18.7% for ACN-based gradients (average of both considered gradient steepness values). When the start and/or end composition lie closer to the viscosity maximum, the analysis time gain becomes smaller as well, thus reflecting that the margin over which the flow rate can be increased becomes smaller. For a 20–80% MeOH gradient for example, the gain is reduced to some 8.3%. For a 40–60% gradient, the potential analysis time advantage of the cP-mode even drops to less than 2%.

The potential gain in analysis time of the cP-mode is further illustrated in Fig. 3, showing a set of simulated cF-mode and cP-mode chromatograms for the case of a linear, volume-based gradient running between 5 and 95% of methanol.

Considering the overlap of the cF- and cP-mode chromatograms in real time units (Fig. 3a), the gain in analysis time obtained by switching to the cP-mode (black chromatogram) is indeed of the order of some 20%, i.e. in agreement with the data shown in Tables 2–3. Similar to what could already be observed in the first example (Fig. 1a and c), Fig. 3a shows that the cP-mode not only accelerates the last eluting compounds but can also accelerate the

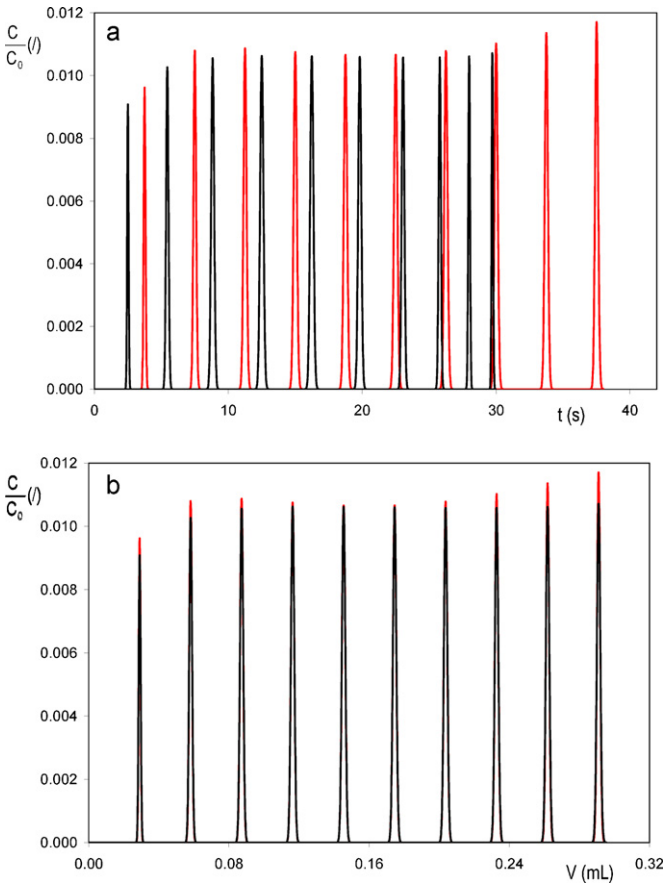


**Fig. 3.** Overlap of cF-mode (red) and cP-mode (black) chromatogram in (a) real time and (b) volume for a volume-based gradient running between 5% and 95% methanol–water (linear gradient, $V_G/V_0 = 9$ in the volume-program mode or $t_G/t_0 = 9$ in the time-program mode). Simulated column length is 1.2 cm and column diameter 2.1 mm, the particle size 2 μm and $\Delta P_{max} = 101.2$ bar, corresponding to $u_0 = 3.2$ mm/s for the cF-mode. (For interpretation of the references to color in text, the reader is referred to the web version of the article.)

early eluting peaks. This is due to the fact that the mobile phase composition in the beginning of a 5–95% methanol–water gradient is still far away from the viscosity maximum, so that the flow rate can also be significantly increased in the beginning of the gradient in the cP-mode.

## 7. Effect of operation mode on separation efficiency

If the efficiency (band broadening) of the separation is not a critical issue (i.e. when the achieved separation resolution is sufficient), the advantage of switching to the cP-mode can readily be quantified from the relative analysis time gains cited in the previous section and in Tables 2–5. However, when the considered cF-mode separation is limited by the resolution of a critical pair or when it suffers from an insufficient peak capacity, also the separation efficiency needs to be taken into account.

Unlike the selectivity, which can be kept identical, small differences in separation efficiency cannot be avoided when switching from the cF-mode to the cP-mode. This can for example be noted from the small differences in peak height between the corresponding peaks in Fig. 3b (compare height of black and red peaks). A similar observation can be made from Figs. S-3b and S-4b of the SM.

As shown by Giddings [2], the separation efficiency is determined by the band broadening, which in turn can be rigorously quantified via the plate height $H$, defined as:

$$H = \frac{\Delta\sigma_x^2}{x} \tag{23}$$

wherein $\Delta\sigma_x^2$ is the increase in spatial variance of the band in the column when its centroid has moved from the inlet to a position located at a distance $x$ from the inlet.

In the literature, there has always been some reluctance towards the use of the plate height concept under gradient conditions because $H$ can only be assessed by estimating the spatial variance from the measured time-based variance which tends to be $(1+k_{loc,e})^2$ times larger than the spatial variance in the column ($k_{loc,e}$ is the local retention factor at the moment of elution) [25]. To correct for this, the value of $k_{loc,e}$ needs to be known and this requires additional measurements or calculations. It is furthermore an additional source of errors. Nevertheless, as shown by Poppe et al. [20], Gritti and Guiochon [21] and recently also by our group [3] and Neue et al. [25], there is no fundamental impediment to continue using the plate height concept under gradient elution conditions.

Doing so, and neglecting in a first instance the effect of peak compression, it can be shown (see SM, Section 1.3 for the detailed derivation) that the effective gradient plate height $H_{eff}$ of a component can be described as a single function of the volumetric gradient program $f_V$ given by [29,30]:

$$H_{eff} = \int_0^{k_{eff,V}+1} \frac{H(f_V(V'))}{1+k_{loc}(f_V(V'))} \cdot dV' \tag{24}$$

Eq. (24) holds without any restriction on the nature of the flow rate (constant or not), and hence holds for both the cF- and the cP-mode case.

In case of an appreciable peak compression, the $H_{eff}$-values need to be corrected by a so-called peak compression factor $G^2$ [17,20–22]. As shown in SM (Section 1.5), the conclusion following from Eq. (24), i.e. that $H_{eff}$ is fully determined by the relative volumetric gradient $f_V$ and is independent of the column length, still holds when accounting for peak compression effects. This could be confirmed via the conducted simulations, since the numerical code automatically also simulates the peak compression effect [3]. An example of a numerical proof is given in SM (Fig. S-6), showing how that the calculated values for the diverse peaks in the chromatogram of the example considered in Fig. 1 indeed vary in a perfectly linear way with $L$.

Since the $H$-expression that needs to be used in Eq. (24) depend on $D_m$, $k_{loc}$ and $u_0$, and it is shown in Section 1.3 of the SM that the analytes will experience the same $k_{loc}$- and $D_m$-history provided the same volume-based gradient program is used, the only difference between a cF- and a cP-mode separation conducted with the same volume-based gradient program is the difference in mobile phase velocity $u_0$. Hence, the expected difference in band broadening between the cP-mode and the cF-mode should be fully determined by the relation between the plate height and the velocity. As advocated by Giddings [31], this relation can most conveniently be represented as a plot of the reduced plate height ($h = H/d_p$) versus the reduced velocity ($\nu = u_0\, d_p/D_m$). It is therefore instructive to first consider how the two variable parameters determining the value of the reduced velocity (i.e. $u_0$ and $D_m$) change during the course of a cF- and a cP-mode run.

For this purpose, Fig. 4a first shows a typical pressure trace for a linear gradient in the cF-mode. According to Darcy's law (see Eq. (5)), this trace is also linearly proportional to the column-averaged viscosity $\bar{\eta}$ (Fig. 4b). Still, according to Darcy's law, the pressure trace is also inversely proportional to the flow rate that can be realized when switching to the cP-mode (see Fig. 4c). Furthermore making the assumption that the gradient is sufficiently flat, so that the local viscosity at the peak center ($\eta_{peak}$) remains close to the column-averaged value $\bar{\eta}$, and assuming that $D_m$ varies inversely proportional with the change in viscosity (i.e. neglecting for example the dependency of the association factors on the mobile phase composition in the Wilke-Chang expression), the local $D_m$-values (Fig. 4d) experienced by the peak during the course of its elution are also inversely proportional to the $P$-trace measured in Fig. 4a.

In the cF-mode, the flow rate and $u_0$ remain constant while $D_m$ will typically follow a trajectory as depicted in Fig. 4d. It can hence be inferred that the reduced velocity, which is proportional to $u_0\, d_p/D_m$, will follow a trajectory that is inversely proportional to $D_m$, i.e. proportional to the $P$-trace depicted in Fig. 4a and the $\eta$-trace depicted in Fig. 4b. An example of the reduced velocity history experienced by the peaks eluting in the cF-mode can be followed from the I–II–III trajectory added to the methanol curve in Fig. 4b. Starting at point I, the reduced velocity will first increase until the viscosity maximum is reached (point II) and will then decrease again to finally reach a new minimum at point III. In the cP-mode on the other hand, both $u_0$ and $D_m$ vary during the course of the elution. They however do so in a more or less parallel way (cf. Fig. 4b and d), at least provided $\eta_{peak}$ and $\bar{\eta}$ do not differ too much. As a consequence, the peak will always experience about the same reduced velocity at any instant during the elution.

The above can be summarized as:

$$\text{cP-mode}: \quad \nu \cong \text{constant} \tag{25a}$$

$$\text{cF-mode}: \quad \nu \leq \nu_{\text{cP-mode}} \tag{25b}$$

The reduced velocity trajectories experienced in both modes are visualized in Fig. 5, for three typical cases of the velocity: a velocity in the B-term dominated range, a velocity near the minimum of the van Deemter curve and a C-term dominated velocity. For the cP-mode, the velocity trajectory reduces to a single dot according to Eq. (25a). Considering the assumptions underlying Eq. (25a), this single dot representation only holds to a first approximation and has only been preferred here for the clarity of the presentation (the single dot approximation was not used during the simulations) and to emphasize the fact that the reduced velocity anyhow varies over a much wider range in the cF-mode. In this mode, the reduced velocity will generally vary from point I over II to III when the mobile phase gradient passes through a viscosity maximum somewhere between its begin and endpoint. If the gradient would incidentally start or end

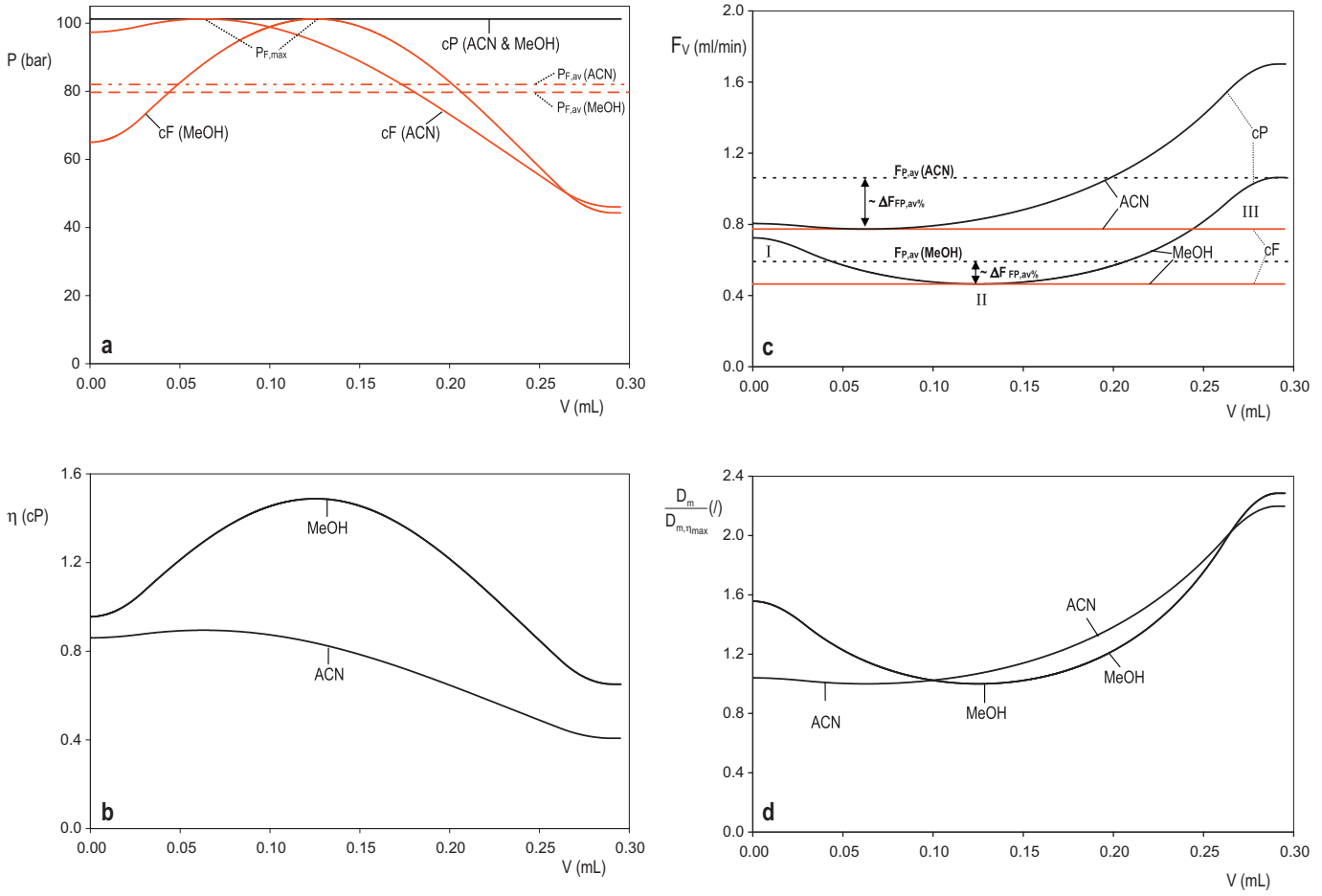


**Fig. 4.** (a) Plot of $\Delta P$ versus pumped volume $V$ in cF-mode (red) and cP-mode (black) for both a 5% and 95% methanol–water and a acetonitrile–water gradient; corresponding plot of (b) $\bar{\eta}$ versus $V$, (c) $F_V$ versus $V$ and (d) $D_m/D_{m,\eta max}$. Same conditions as in Fig. 3. (For interpretation of the references to color in text, the reader is referred to the web version of the article.)

with a mobile phase with a maximal viscosity, only trajectory I to II (maximal viscosity at start of gradient) or II to III (maximal viscosity at end of gradient) remain. In any case, the reduced velocity experienced by a given peak is in the cF-mode always smaller than in the cP-mode, so that the dot representing the cP-mode operation is always situated at the highest velocity along the I–II–III trajectory.

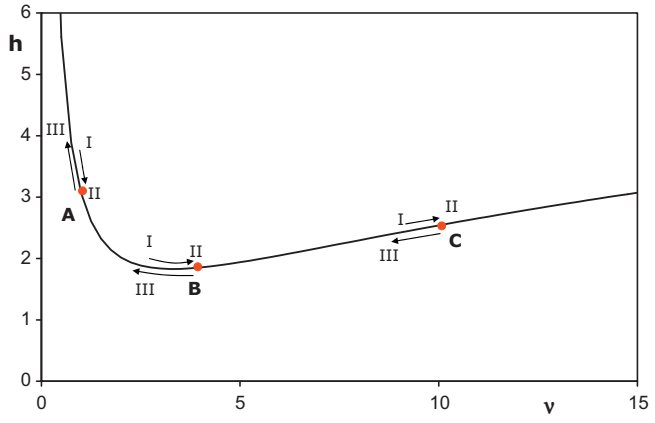


**Fig. 5.** Schematic view of a reduced van Deemter curve and a representation of the typical reduced velocity trajectory followed in the cP-mode (red dots) and the cF-mode (I–II–III trajectory). (For interpretation of the references to color in text, the reader is referred to the web version of the article.)

As can be readily noted from Fig. 5, the difference in efficiency between the cP- and cF-mode depends on the range of velocities the column is operated in. In the C-term regime (point C), the cF-mode will provide a better separation efficiency, because the average $h$-value along the I–II–III trajectory (cF-mode) is in this velocity range consistently smaller than the (constant) $h$-value experienced in the cP-mode (represented by the red dot). The inverse of course happens when the column is operated in the B-term regime (point A). Here the smaller velocities of the cF-mode operation (I–II–III trajectory) lead to a significant increase of the local plate heights compared to the plate height at the red dot representing the cP-mode operation. Finally, for separations operated close to the minimum of the van Deemter curve (point B), it can be expected that the difference in band broadening between the cP- and the cF-mode will be very small and virtually non-existing.

This is confirmed in the zoom-in chromatograms (showing only the last two eluting peaks of the separation shown in Fig. 3) shown in Fig. 6. In Fig. 6a, the applied pressure and flow rate were relatively small so that the peaks continuously experienced a velocity well-below the optimal velocity, similar to point A in Fig. 5. As can be noted, the cP-mode peaks (colored in black) are slightly taller and narrower than in the cF-mode (in red), thus reflecting the smaller band broadening they have been subjected to. This effect was most significant for the early (results not shown) and the late eluting compounds (shown in Fig. 6) in the chromatogram, because here the difference in average mobile phase velocity between the cF- and cP-mode is largest (cf. regions I and III in Fig. 4c). For gradients running from 5 to 50% MeOH, where the difference in velocity

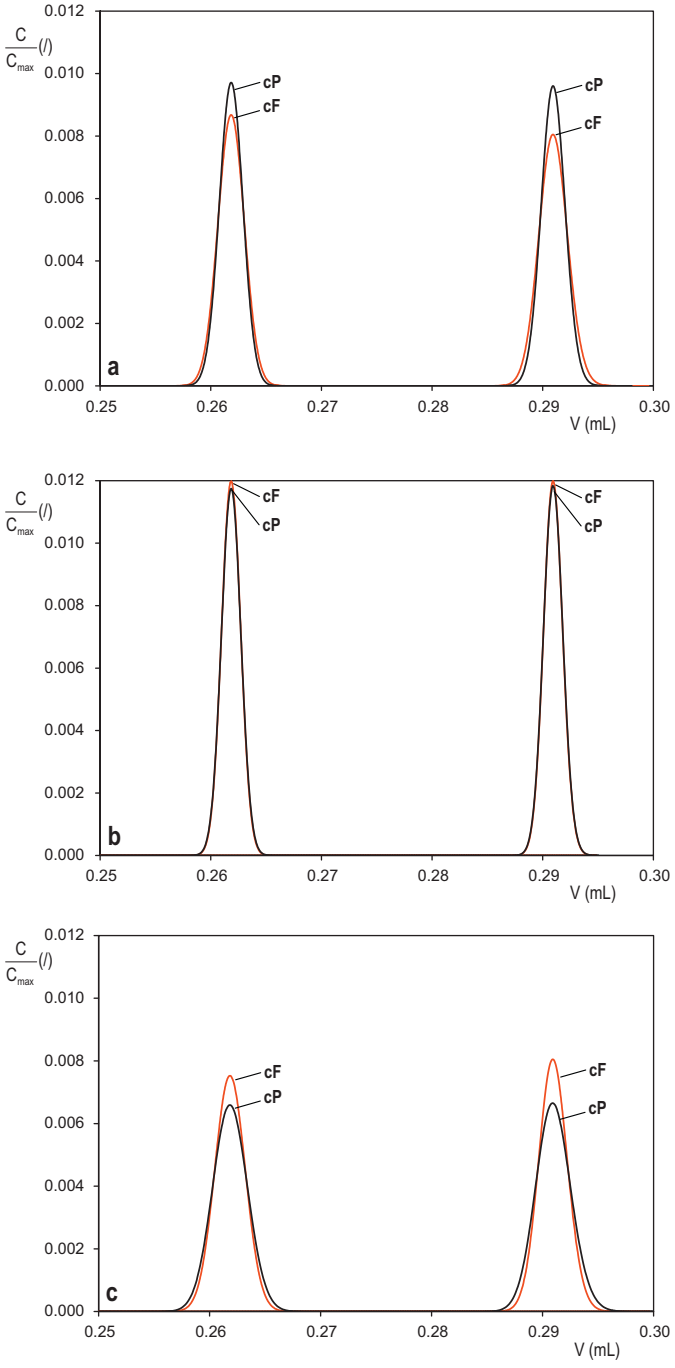


**Fig. 6.** Overlap of cF-mode (red) and cP-mode (black) chromatogram of the two last eluting compounds ($k$ = 8 and 9) for a volume-based gradient running between 5% and 95% methanol–water (linear gradient, $V_G/V_0$ = 9 in the volume-program mode or $t_G/t_0$ = 9 in the time-program mode) for three different cP-mode operating pressures (a) $\Delta P_{max}$ = 10 bar, corresponding to $u_0$ = 0.32 mm/s for the cF-mode; (b) $\Delta P_{max}$ = 50 bar, corresponding to $u_0$ = 1.6 mm/s for the cF-mode and (c) $\Delta P_{max}$ = 600 bar, corresponding to $u_0$ = 19.2 mm/s for the cF-mode. Simulated column length is 1.2 cm and ID = 2.1 mm. (For interpretation of the references to color in text, the reader is referred to the web version of the article.)

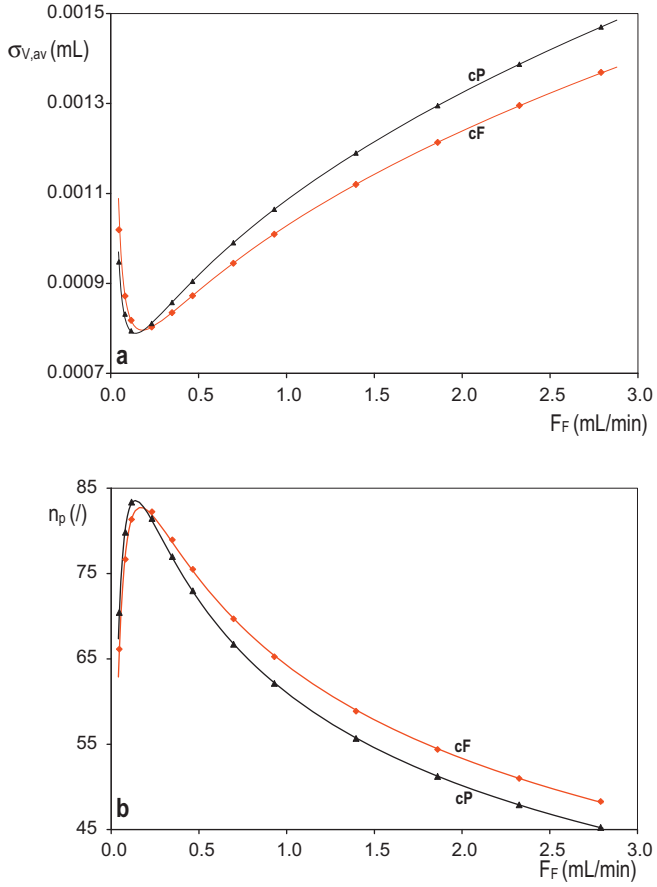


**Fig. 7.** (a) Evolution of the volumetric peak standard deviation $\sigma_V$ as a function of the mobile phase flow rate $f_V$ (mL/min) for cF- (red) and cP-mode (black) for fixed length (=1.2 cm) column. (b) Corresponding values of the peak capacity as a function of flow rate. Other conditions the same as Fig. 3. (For interpretation of the references to color in text, the reader is referred to the web version of the article.)

between the cP- and the cF-mode is only pronounced at the beginning of the gradient, the improved efficiency of the cP-mode was most pronounced for the early eluting compounds. Similarly, an improved efficiency is only noted for the late eluting compounds for gradients of 50–95% methanol (results not shown).

Considering a velocity close to the optimum velocity (Fig. 6b) the difference in band broadening is clearly much smaller than in Fig. 6a. This is in full agreement with the fact that the difference in plate heights between a cP- and cF-mode operation is anyhow small near the optimum velocity (cf. point B of Fig. 5). When the covered range of velocities is fully situated in the C-term dominated regime (cf. point C of Fig. 5), as is the case for the separation represented in Fig. 6c, the cF-mode yields narrower peaks than the cP-mode. This is again in full agreement with the observation that can be made from Fig. 5, showing that the I–II–III trajectory followed in the cF-mode in the C-term range leads to smaller $h$-values than the $h$-value corresponding to the single dot velocity of the cP-mode. Once again, this effect is more pronounced for the late eluting compounds for gradients running from 50 to 95% methanol (see SM, Fig. S-5a on the right hand side) on the one hand and for the early eluting compounds for gradients from 5 to 50% (see SM, Fig. S-5b on the left hand side).

The efficiency of the chromatograms shown in Fig. 6 (and of some additional cases with a different velocity) are further quantified in Fig. 7a, showing how $\sigma_{V,av}$, the volumetric band standard deviation averaged over all the individual peaks of the chromatogram, varies as a function of the flow rate. Since it is difficult to define a characteristic flow rate for the cP-mode operation ($F$ is not a constant), the cP-mode data have simply been plotted versus the $F$-value of the corresponding cF-mode case (same $\Delta P_{max}$). Although this $F$-value is only an approximation of the true velocity history in the cP-mode, it perfectly suits the purpose of visualizing the trend that was already visible in the chromatograms shown in Fig. 6: the cP-mode produces narrower bands than the cF-mode in the range of sub-optimal flow rates, whereas the opposite is true in the range

of low flow rates above the optimal flow rate. The cP- and cF-mode curves shown in Fig. 7a also clearly display the typical van Deemter behavior: $\sigma_{V,av}$ decreases steeply with $F$ in the low velocity region (B-term behavior), then goes through a minimum (thus fixing the value of the optimal flow rate), and subsequently increases again with $F$ in the high velocity region (C-term behavior).

Approximating the $h$-curve underlying the observations made in Figs. 6 and 7 with the basic van Deemter model, for which:

$$h = A + \frac{B}{v} + C \cdot v \tag{26}$$

the above findings can be rationalized in a simplified form by stating that the relative change in $h$ ($\Delta h_{\%}$) resulting from the switch from a cF- to a cP-operation is directly related to the average increase in flow rate and pressure as:

- in B-term dominated regime:

$$\Delta h_{\%} \sim \frac{1}{\Delta F_{av\%}} \sim \frac{1}{\Delta P_{av\%}} \left(\text{since } h \sim \frac{1}{v}\right) \tag{27a}$$

- around velocity optimum:

$$\Delta h_{\%} \cong 0 \,(\text{since } h \text{ is independent of } v) \tag{27b}$$

- in C-term dominated regime:

$$\Delta h_{\%} \sim \Delta F_{av\%} \sim \Delta P_{av\%} \,(\text{since } h \sim v) \tag{27c}$$

## 8. Combined effect: comparison of the peak capacity and the kinetic performance limit of cF-mode and cP-mode operations

The obvious measure combining selectivity (discussed in Section 4) and efficiency (discussed in Section 7) is the separation resolution $R_s$. In a volume-based chromatogram, $R_s$ is defined as:

$$R_{s,V} = \frac{V_{R,i} - V_{R,i-1}}{4 \cdot (\sigma_{V,i} + \sigma_{V,i-1})/2} \tag{28}$$

wherein $i$ and $i-1$ are the annotation numbers of two successive peaks. Since only the volume-based chromatogram provides the correct separation information in the cP-mode (see Section 3.3), the resolution that would be measured in a time-based chromatogram is not considered here. On the other hand, the resolution one would measure in a time reconstructed-chromatogram as the one represented in Fig. 2b would correspond exactly to that determined by Eq. (28), because this chromatogram is obtained by a perfectly linear rescaling of the volume-based chromatogram.

Typically, the resolution value would be reported for the critical pair of the chromatogram. When discussing the performance of different chromatographic systems under gradient elution conditions, it has however become more customary to report the peak capacity. Although many different definitions exist, the most correct estimate of the column peak capacity one can read out from a chromatogram is that based on the sum of the resolution values of each subsequent peak pair [32,33]

$$n_p = 1 + \sum_{i=1}^{n_c} R_{S,V,i} = 1 + \sum_{i=1}^{n_c} \frac{V_{R,i} - V_{R,i-1}}{2 \cdot (\sigma_{V,i} + \sigma_{V,i-1})} \tag{29}$$

Eq. (29) is indeed the closest one can get to the exact integral definition of peak capacity (see e.g. Eq. (1) in Ref. [33]). A number of possible variants can be derived from Eq. (29). One could leave out the peak with $i=0$ (dead volume marker), in which case $n_p$ is only counted starting from the first sample peak, and/or one could add an extra term covering the space between the last eluting compound and the point where the end of the gradient elutes from the column.

In the present study, the question whether the $n_p$-value should best be based on either $t_G$ or on $(t_{R,\text{last}} - t_0)$ or on $(t_{R,\text{last}} - t_{R,\text{first}})$ has been simply circumvented by tuning the retention properties of the components of the numerical sample such that they would cover the complete elution window, having retention volumes ranging between $V_0$ and $V_0 + V_G$.

Fig. 7b shows the peak capacity calculated using Eq. (29) for the simulated chromatograms that were also used to establish Fig. 7a. In agreement with the effects observed in Fig. 7a, Fig. 7b shows that the cP-mode can be expected to lead to a smaller peak capacity in the high velocity or flow rate range (C-term dominated regime), whereas the opposite would occur in the low velocity range (B-term dominated regime).

A drawback of the peak capacity plot in Fig. 7b is that it provides no direct information about the speed of the separation or the kinetic performance limits of the technique. This information is hidden in the flow rate and in the unused pressure potential (all but the highest flow rate data points relate to conditions where the pressure is sub-maximal). To circumvent this problem, and transform each different data points of either Fig. 7a or 7b into a data point lying at the kinetic performance limit (KPL), the so-called kinetic plot theory can be used [3–5,34–36]. According to this theory, recently extended gradient elution conditions [3], this transformation can be done using the so-called column length rescaling factor $\lambda$:

$$\lambda = \frac{\Delta P_{col,\max}}{\Delta P_{col,\exp}} \tag{30}$$

This $\lambda$ is a readily obtainable experimental parameter. The value of $\Delta P_{col,\exp}$ is the maximum column pressure drop experienced during the gradient run (in the cP-mode this is simply the operating pressure), whereas $\Delta P_{col,\max}$ is the pressure maximum of the column or the pump. This $\lambda$-value (note that each considered experimental velocity leads to a different value) can then be applied in below transformation expressions to turn the experimentally measured $t_{R,\exp}$ and $n_{p,\exp}$ into their corresponding values at the KPL of the system [3]:

$$t_{R,KPL} = \lambda \cdot t_{R,\exp} \tag{31}$$

$$n_{p,KPL} = 1 + \sqrt{\lambda} \cdot (n_{p,\exp} - 1) \tag{32}$$

As shown in [3], the only condition underlying the validity of the KPL-transformation is that $k_{eff,V}$ and $H_{eff}$ should be independent of the column length. The theoretical derivations presented in Sections 4 and 7 show that the column length only interferes in the expression for both $k_{eff}$ (see Eq. (S-13) in the SM) and $H_{eff}$ (Eq. (24)) via the reduced volume $V'$ (with $V'$ = pumped volume/$V_0$ and $V_0 = \varepsilon_T A L$). Since Eqs. (S-13) and (24) furthermore only depend on $f_V(V')$, one can hence expect to find the same value for $k_{eff}$ and $H_{eff}$ provided the same $f_V(V')$-program is run on each different length columns. Under this condition, even the degree of peak compression can be expected to be identical (see SM, Section 1.5). Since running the same $f_V(V')$-program corresponds to keeping the gradient program identical in reduced volumetric coordinates, the condition to obtain identical $k_{eff,V}$- and $H_{eff}$-values only requires that the characteristic volumes $V_a$, $V_b$, etc. appearing in the gradient program are linearly scaled with the column length so as to maintain the same dimensionless values of $V'_a$, $V'_b$, etc. (with $V'_a = V_a/V_0$, $V'_b = V_b/V_0$, etc.). This condition is in agreement with the conditions proposed for the length-independency of $k_{eff,V}$ by Snyder and Dolan [37] and Jandera [14].

Since the expressions for $k_{eff,V}$ and $H_{eff}$ established in Sections 4 and 7 did not require to assume that the flow rate is kept constant, it can be concluded that the KPL-transformation equations given by Eqs. (30)–(32), originally established in [3] for the cF-mode, should also hold in the cP-mode.

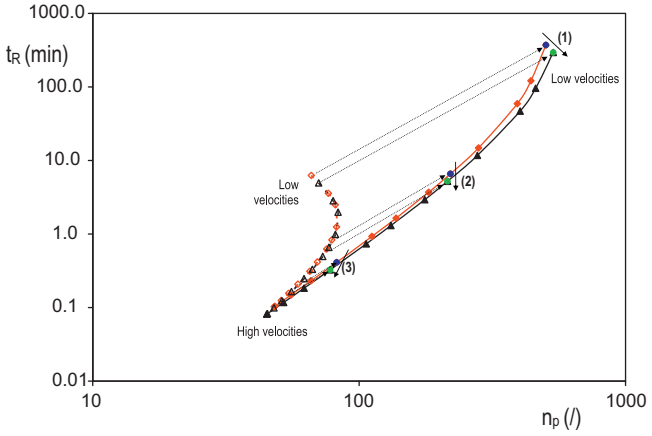


**Fig. 8.** Kinetic plot showing the total required analysis time $t_R$ as a function of the required peak capacity ($n_p$) for cF (red squares) and cP operation (black triangles) for a fixed length column (=1.2 cm) (open symbols, dotted lines) and the corresponding kinetic performance limit (KPL, $\Delta P_{col,max}$ = 600 bar, full symbols, full lines). Same conditions as Fig. 3. The meaning of the arrows is discussed in the text. (For interpretation of the references to color in text, the reader is referred to the web version of the article.)

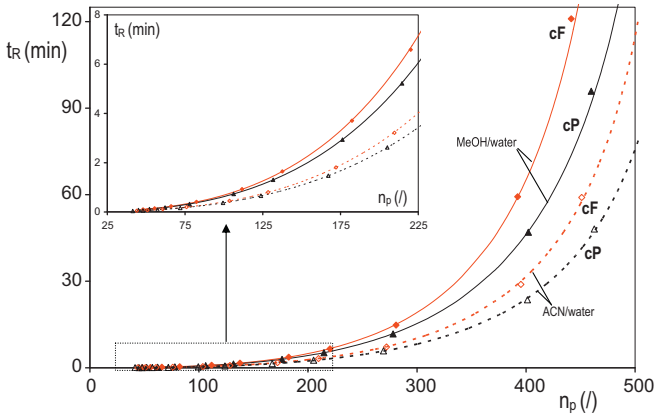


**Fig. 9.** Kinetic plot showing the KPL of Fig. 8 in linear axis for constant flow (red squares) and constant pressure (black triangles) for an acetonitrile–water gradient (open symbols, dotted lines) and a methanol–water gradient (full symbols, full lines) both running from 5 to 95%. (For interpretation of the references to color in text, the reader is referred to the web version of the article.)

The graphical representation of the establishment of the KPL-curve for the simulated cF- and cP-mode separations is shown in Fig. 8. The dashed curves represent the fixed length column data relating to the simulations already represented in Fig. 7. The full line curves were obtained via the KPL-transformation using Eqs. (30)–(32), whereas the blue and green dot data were obtained by redoing the simulations on a column with a different length and operating at the maximal pressure, but with the same flow rate and using the same gradient program in reduced volumetric coordinates as the original column. As can be noted, the agreement between the KPL-prediction and the actual performance measured on the different length columns is perfect, despite the complex peak compression and variable flow rate effects. This agreement hence provides a clear numerical proof for the validity of the KPL-theory under cP-mode operation conditions, similar to that delivered in [3] for the cF-mode (see Section 9 for the adopted assumptions).

The two KPL-curves (solid lines) in Fig. 8 provide a comprehensive view of the kinetic advantage of the cP-mode for the case of a 5–95% water-methanol gradient. The cP-mode curve everywhere lies below the cF-mode curve, indicating a better kinetic performance, although the difference vanishes towards the left bottom corner of the plot, i.e. for separations conducted in the C-term dominated regime [4,36]. Progressively moving upward along the curve, the flow rate relating to the different data points progressively decreases until the most rightward data point is reached, usually situated in the B-term dominated regime. Fig. 8 hence shows that the largest advantage for the cP-mode would be observed when operating in the B-term regime. This is however a range that is seldom used in practice, because it is in this case always possible to reduce the analysis time by switching to a larger particle size.

Investigating the difference between the cF- and the cP-mode curves in more detail, the effect of the prevailing (average) flow rate on this difference can readily be understood from the arrows added to Fig. 8. These arrows indicate how the KPL shifts when switching from the cF- to the cP-mode for a selected number of different flow rate cases. Since the selectivity does not change when switching from the cF- to the cP-mode, the observed shifts are exclusively due to a reduction of the analysis time and/or a difference in band broadening (represented here in terms of the peak capacity). The direction of the arrows hence always consists of a time reduction component (downward shift, directly proportional to $\Delta F_{av,\%}$, see Eq. (21)) and a component representing the change in peak capacity originating from the difference in band broadening (horizontal shift). In the B-term dominated regime (arrow 1), the net result of both changes leads to a double gain (arrow shifts towards lower right corner): $h$ decreases with $\Delta P_{av,\%}$ (see Eq. (27a)) and the total analysis time also decreases with $\Delta P_{av,\%}$. Near the optimum velocity (arrow 2), the arrow shifts purely downward because its horizontal component, representing the difference in $h$, is virtually zero (see Eq. (27b)). In the C-term dominated regime (arrow 3), the arrow shifts downward (over a distance that is again proportional to $\Delta P_{av,\%}$) but also to the left (because now $h$ increases with $\Delta P_{av,\%}$, see Eq. (27c)). When both effects are equally strong (which will occur when the flow rate is situated deep enough in C-term range so that Eq. (27c) holds), they will cancel out, explaining the fact that the cP-mode and the cF-mode curve slowly tend towards each other in the C-term dominated part of the KPL-curve.

This implies that the cP-mode is only really beneficial (with net relative gains in the order of the values cited in Tables 2–5) for separations conducted in columns that operate near the optimal flow rate when being subjected to the maximal pressure. This is however a condition with a high practical relevance because it is the condition for which any type of chromatographic particles achieves its kinetic optimum, i.e. the so-called Knox and Saleem limit [1]. Using Knox' optimal performance expressions [38] with $\phi$ = 800, $\nu_{opt}$ = 3 and $h_{min}$ = 2, and considering the case of 2 μm particles, a compound with $D_m = 10^{-9}$ m$^2$/s and a maximal operating pressure of 1200 bar, it is found that the kinetic optimum is achieved in columns with a length of about 10–15 cm and lasting about 30 min (assuming the last component elutes around $k_{eff,V}$ = 10) when using methanol-based gradients (assuming $\eta_{av}$ = 1.2cP) and also about 10–15 cm long and lasting about 20 min when using acetonitrile-based gradients (assuming $\eta_{av}$ = 0.7cP and assuming $D_m$ reduces in proportion to $\eta_{av}$).

The potential kinetic advantage of the cP-mode operation can be quantified in more detail from Fig. 9, where the KPL-curves shown in Fig. 8 are now represented in linear coordinates and where also a zoom-in of the lower range of the curve is provided. As can be noted, the kinetic advantage of switching to the cP-mode is very similar for the acetonitrile–water gradient (dashed line curves) and the water-methanol gradient (full line curves), at least for the presently considered 5–95% gradient span. The fact that the acetonitrile–water data lie to the right of the methanol–water data, and thus provide a better kinetic performance, is a direct consequence of the lower viscosity of the former.

Another way to compare the kinetic performance of the cF and cP-mode is given in Fig. S-7 in the SM, which represents the rela-

tive gain in analysis time as a function of the desired peak capacity. In other words, this graph gives an indication on how far the KPL curves in Fig. 8 and 9 lie apart vertically. The curve presented there show that the gain in analysis time for a given efficiency is lower than those given in Tables 2–5 for short analysis times (C-term operation), but becomes larger than expected for higher analysis times (B-term operation). Once again, this is due to the fact that the kinetic plot method incorporates the effect of both the analysis time and the efficiency.

## 9. Some remarks concerning the adopted assumptions

The results in the preceding sections were all obtained by assuming isothermal operation conditions and assuming that the viscosity and the local retention factor are pressure-independent. These assumptions however clearly do not hold under ultra-high pressure conditions. In this case, the inevitable viscous heating automatically leads to a non-isothermal operation, with the development of both spatial and temporal (because of the varying mobile phase composition) temperature gradients. There is furthermore also abundant experimental evidence and theoretical proof that the viscosity and the retention factor can no longer be considered as constant under ultra-high pressure conditions [7,39,40].

In the discussion of the adopted assumptions, we will first consider the two operation modes separately and focus on only one of the conditions underlying the validity of the kinetic plot method, i.e. that the viscosity is independent of the column length or the employed pressure. Doing so, it is first of all important to realize that the developed viscous friction heat is determined by both the viscosity and the pressure evolution inside the column [41]. However, the pressure is a given constant in the cP-mode, whereas its evolution is fully determined by the viscosity in the cF-mode. As a consequence, it can be said that the generated viscous heat is exclusively determined by the viscosity. Since it can be inferred that the pattern with which the viscosity will vary as a function of the relative time (or the relative run volume) will be independent of the column length provided the same gradient program is imposed in dimensionless volumetric units, it can also be expected that the relative viscous heating history of the separation will be identical as well. The elevated pressure and viscous heating effects affecting the mobile phase viscosity during the measurement of the highest velocity data point on the fixed-length column will hence also occur in any different length columns that is subjected to the same gradient program. As a consequence, it can be inferred that the effect of the elevated pressure and the concomitant viscous heating on the mobile phase viscosity can be properly taken into account by basing the entire KPL-transformation on the viscosity observed during the measurement of the highest velocity data point on the fixed-length column. Using similar argumentation, it can be inferred that the same approach (i.e. use the retention factor observed when measuring the highest velocity data point) should be adopted for the effective retention factor $k_{eff}$.

The above considerations for $\eta$ and $k_{eff}$ are identical to those already formulated for the constant flow rate gradient kinetic plot in the SM of [3], where it was stated that, in order to account for ultra-high pressure and viscous heating effects on $\eta$, the $\lambda$-factor defined in Eq. (30) should in fact be written as:

$$\lambda(F) = \lambda_{F_{\max}} \cdot \frac{F_{\max}}{F} \tag{33}$$

while a factor $(1 + k_{eff,F_{\max}})/(1 + k_{eff})$ should be added to the right hand side of Eq. (31) to properly calculate the retention times that can be expected when the KPL is calculated for the highest possible operating pressure.

A moderating remark that should be made is that the above only holds provided the thermal boundary conditions do not change with the column length. The latter would pose no problem provided it would be possible to operate the columns in a perfectly thermostatted or perfectly adiabatic mode. In practice, however, these idealized conditions are difficult to realize and it might hence be that the thermal conditions will vary slightly with the column length because of the changing ratio of column endfittings to column mantle surface or because of the use of coupled column systems. Such changes have indeed already been reported [42] and will introduce a small length dependency on the observed $H_{eff}$ and $k_{eff}$.

Another requirement underlying the validity of the KPL-transformation is that the effective plate height should be independent of the applied pressure and the concomitant viscous heating. This is a requirement that obviously cannot be met exactly, because the plate height depends on the diffusion coefficient and the retention factor (cf. Section 1.3 of the SM) and these are in general pressure- and temperature-dependent. However, both parameters have an opposite effect on both the diffusion coefficient and the retention factor, so that their effect to some extent compensates for one another, at least when the thermal boundary conditions of the column are close to adiabatic [41]. This condition is satisfied for columns hanging in a still-air oven, but not for forced-air ovens, where it is well-known that viscous heating can lead to very steeply increasing plate height curves in the C-term regime [42–44]. Obviously, the compensation of the effect of pressure and temperature on the plate heights can never be exact, not even under perfectly adiabatic conditions, and will hold better for one class of components than for another. Nevertheless, the effect generally remains limited up to pressures of 1000–2000 bar [41] so that the KPL-extrapolation can still be done within a reasonable range of accuracy. The problem that pressure and viscous heating lead to a non-exact KPL-extrapolation is not unique to cP-operations, but also shows up to the same extent for isocratic separations as well as for cF-gradient elution separations. In both cases, the accuracy of KPL-extrapolation has already been experimentally investigated up to pressures of 600 bar (gradient elution) [3] and 1000 bar (isocratic elution) [42] on typical commercial instruments (both forced and still air ovens) and columns. In any case, it was found that the extrapolation error was always less than 10% (less than 3% for isocratic separations in a still-air oven). This error was mainly due to differences in thermal conditions (it is difficult to maintain the same thermal boundary conditions if going form a single short column to longer and or coupled column systems), as well as to the fact that the employed different-length columns already intrinsically had a slightly different efficiency, apart from any pressure or viscous heating issues [3,42].

Turning now to the effect of ultra-high pressures on the comparison of the cP- and the cF-mode, it should be recognized that both modes inevitably display a different pressure trajectory ($P = P_{\max}$ in the cP-mode, whereas pressure varies quite strongly with the time in the cF-mode). As a consequence, differences in the effect of viscous heating and high pressures on the mobile phase viscosity and the effective retention factor of the analytes are difficult to avoid. Nevertheless, because viscous heating and elevated pressures have an opposite effect on $\eta$ and $k_{eff,V}$, it can be expected that the net effect will remain relatively small. This can be understood as follows. Typically, the maximal difference in average pressure between the cP- and the cF-mode will lie around 20% (highest values in Tables 2–5). Such a difference in pressure can be expected to gives rise to some 4% increase in viscosity. However, because of the higher operating pressure, also the viscous heating will be significant. Given that most columns are relatively close to adiabatic conditions, and given that the effect of temperature on the viscosity is larger than that of pressure, the net effect of the higher operating pressure in the cP-mode can be expected to lead to a net reduction of the viscosity (only this effect will be very small, below

1%, as a rough estimate). Nevertheless, this reduction implies that the cP-mode can be expected to produce even slightly higher flow rates (and hence shorter analysis times than those predicted on the basis of the isobaric and isothermal assumptions made in Section 6 and leading up to Tables 2–5). Similar argumentation can be followed for the effective retention factor. For most small molecular weight compounds, the net effect of pressure and viscous heating also tends towards a reduction of $k_{eff}$ with increasing inlet pressure, so that one can expect that the $k_{eff}$-values in the cP-mode might be somewhat smaller than in the cF-mode. This would lead to an additional reduction of the elution time of the last eluting compound. However, this effect is not entirely positive, since it would also imply a reduction of the sample-based peak capacity (because of the reduction of the available retention window). The change would certainly also lead to differences in selectivity, but this can turn out either positively or negatively depending on the nature of the compounds.

The above considerations certainly need to be investigated more in-depth in a follow-up study. The conclusions of this study can be expected to be highly complex, not only because they will depend on the nature of the sample compounds, but also because the temperature trajectory in the column inevitably depends highly on the thermal boundary conditions (which in practice are difficult to control and describe) as well as on the events preceding the actual separation, because, due to the thermal inertia, part of the temperature profile in the column is always reminiscent of the heating or cooling effects occurring during the preceding run or the preceding column preconditioning run.

## 10. Conclusions

Provided both modes are run with the same reduced volume-based gradient program, the constant-pressure (cP) mode can offer an identical separation selectivity as the constant-flow (cF) rate mode (except from some small differences induced by the difference in pressure and viscous heating trajectory). Depending on the start and end composition of the gradient mixture, the cP-mode can obtain this given selectivity in a shorter time. The potential time gain can be expected to depend only weakly on the slope of the gradient and on the nature of the organic modifier. The gain can also be expected to be directly proportional to the relative increase in average operating pressure $\Delta P_{av\%}$ that can be realized by switching to the cP-mode. As a consequence, the gain will be largest for gradients covering the largest span in mobile phase viscosity (this range runs between 50 and 95% for methanol/water and between 20 and 95% for acetonitrile/water). For a typical scouting gradient running between 5 and 95% of organic modifier, the relative time gain for the execution of a complete linear gradient program can be expected to be of the order of some 20% for both methanol–water and acetonitrile–water systems. Smaller gains can be expected when the start and end composition lie closer to the viscosity maximum of the considered water-organic modifier system.

Operating under variable flow rate conditions, as is the case in the cP-mode, the recorder signal should no longer be plotted as a function of the time but as a function of the pumped volume, as the former does not correctly represent the actual separation resolution that is achieved inside the column. If desired, the transition between time and volume coordinates can be “softened” in the mind of the practitioner by introducing a reconstructed time axis (see Section 5). This reconstruction is very straightforward, as it only requires that the actual run volume is divided by a nominal flow rate.

Programming gradients as a function of the volume in such a way that they produce the same selectivity as a time-based gradient program run in the cF-mode is straightforward and can proceed via the very simple Eq. (9). The resulting expressions for the effective retention factor and the retention factor at the moment of elution in the case of a linear gradient for example remain fully similar to those obtained for a time-based linear gradient (see Eqs. S-34 and S-35 in the SM).

The condition of an identical reduced volume-based gradient program is also the only necessary condition to obtain effective gradient plate heights that are independent of the column length and to allow for a reliable kinetic performance limit (KPL) extrapolation. This even holds when taking the effect of peak compression into account (see Section 1.5 in the SM). Although the length-independency of $H_{eff}$ and $k_{eff}$, as well as the validity of the KPL-extrapolation might be might be affected by ultra-high pressure and/or viscous heating effects on the viscosity of the mobile phase and on the retention coefficients of the compounds, it can be inferred that these effects remain relatively small for the currently available operating pressures.

The cF- and cP-operation mode may lead to small differences in separation efficiency, depending on whether they are compared on the basis of a flow rate situated in the B-term or the C-term range of the van Deemter curve. In the B-term range, the cP-mode leads to an additional decrease of the band broadening, in proportion with the inverse of $\Delta P_{av\%}$. In the C-term dominated regime, the width of the bands increases in proportion to $\Delta P_{av\%}$ so that in this regime the cF-mode offers the best efficiency when comparing both systems for the same pressure. Around the minimum of the van Deemter curve, both operation modes lead to a similar efficiency.

Combining the effect on the elution time and the efficiency into a kinetic plot representing the maximal peak capacity versus time, it turns out that both modes perform as well in the full C-term dominated regime, while the cP-mode has a clear advantage for operations that are run around the van Deemter or in the B-term dominated regime, where the gain is maximal. Near the optimal flow rate, and for linear gradients running from 5 to 95% organic modifier, time gains of the order of some 20% can be expected (or 25–30% when accounting for the fact that the cP-mode can be run without having to leave a pressure safety margin of 5–10% as is needed in the cF-mode).

## Acknowledgements

K.B. and M.V. gratefully acknowledge research grants from the Research Foundation – Flanders (FWO Vlaanderen).

## Appendix A. Supplementary data

Supplementary data associated with this article can be found, in the online version, at 10.1016/j.chroma.2010.12.086.

## References

[1] J.H. Knox, M. Saleem, J. Chromatogr. Sci. 7 (1969) 614.
[2] J.C. Giddings, Dynamics of Chromatography – part 1, Marcel Dekker, New York, USA, 1965.
[3] K. Broeckhoven, D. Cabooter, F. Lynen, P. Sandra, G. Desmet, J. Chromatogr. A 1217 (2010) 2787.
[4] G. Desmet, D. Clicq, P. Gzil, Anal. Chem. 77 (2005) 4058.
[5] U.D. Neue, LC–GC Eur. 22 (2009) 570.
[6] P.W. Carr, X.L. Wang, D.R. Stoll, Anal. Chem. 81 (2009) 5342.
[7] J. Billen, K. Broeckhoven, A. Liekens, K. Choikhet, G. Rozing, G. Desmet, J. Chromatogr. A 1210 (2008) 30.
[8] D. Guillarme, S. Heinisch, J.L. Rocca, J. Chromatogr. A 1052 (2004) 39.
[9] H. Colin, J.C. Diez-Masa, G. Guiochon, T. Czjkowska, I. Miedziak, J. Chromatogr. 167 (1978) 41.
[10] J.W. Li, P.W. Carr, Anal. Chem. 69 (1997) 2550.
[11] E.C. Freiling, J. Phys. Chem. 61 (1957) 543.
[12] B. Drake, Ark. Kemi. 8 (1955) 1.
[13] P. Nikitas, A. Pappa-Louisi, Anal. Chem. 77 (2005) 5670.
[14] P. Jandera, J. Chromatogr. A 1126 (2006) 195.

[15] M. Martin, J. Liq. Chromatogr. 11 (1988) 1809.
[16] L.R. Snyder, J. Chromatogr. 13 (1964) 415.
[17] L.R. Snyder, D.L. Saunders, J. Chromatogr. Sci. 7 (1969) 195.
[18] L.R. Snyder, J.W. Dolan, J.R. Gant, J. Chromatogr. 165 (1979) 3.
[19] P. Jandera, J. Churacek, J. Chromatogr. 91 (1974) 223.
[20] H. Poppe, J. Paanakker, M. Bronckhorst, J. Chromatogr. 204 (1981) 77.
[21] F. Gritti, G. Guiochon, J. Chromatogr. A 1212 (2008) 35.
[22] U.D. Neue, D.H. Marchand, L.R. Snyder, J. Chromatogr. A 1111 (2006) 32.
[23] F. Gritti, G. Guiochon, J. Chromatogr. A 1145 (2007) 67.
[24] P.J. Schoenmakers, H.A.H. Billiet, R. Tijssen, L. de Galan, J. Chromatogr. 149 (1978) 519.
[25] U.D. Neue, H.B. Hewitson, T.E. Wheat, J. Chromatogr. A 1217 (2010) 2179.
[26] A. Pappa-Louisi, P. Nikitas, A. Zitrou, Anal. Chim. Acta 573–574 (2006) 305.
[27] P. Nikitas, A. Pappa-Louisi, K. Papachristos, C. Zisi, Anal. Chem. 80 (2008) 5508.
[28] K. Papachristos, P. Nikitas, J. Chromatogr. A 1216 (2009) 2601.
[29] G. Desmet, K. Broeckhoven, Anal. Chem. 80 (2008) 8076.
[30] U.D. Neue, J. Chromatogr. A 1079 (2005) 153.
[31] J.C. Giddings, J. Chromatogr. 13 (1964) 301.
[32] J.C. Giddings, Unified Separation Science, Wiley/Interscience, New York, 1991.
[33] U.D. Neue, J. Chromatogr. A 1184 (2008) 107.
[34] T.J. Causon, E.F. Hilder, R.A. Shellie, P.R. Haddad, J. Chromatogr. A 1217 (2010) 5057.
[35] T.J. Causon, E.F. Hilder, R.A. Shellie, P.R. Haddad, J. Chromatogr. A 1217 (2010) 5063.
[36] G. Desmet, D. Clicq, D.T.-T. Nguyen, D. Guillarme, S. Rudaz, J.-L. Veuthey, N. Vervoort, G. Torok, D. Cabooter, P. Gzil, Anal. Chem. 78 (2006) 2150.
[37] L.R. Snyder, J.W. Dolan, Adv. Chromatogr. 38 (1998) 115.
[38] J.H. Knox, J. Chromatogr. Sci. 18 (1980) 453.
[39] M.M. Fallas, U.D. Neue, M.R. Hadley, D.V. McCalley, J. Chromatogr. A 1209 (2008) 195.
[40] M.M. Fallas, U.D. Neue, M.R. Hadley, D. McCalley, J. Chromatogr A 1217 (2010) 276.
[41] U.D. Neue, M. Kele, J. Chromatogr. A 1149 (2007) 236.
[42] D. Cabooter, F. Lestremau, A. de Villiers, K. Broeckhoven, F. Lynen, P. Sandra, G. Desmet, J. Chromatogr. A 1216 (2009) 3895.
[43] M.M. Fallas, M.R. Hadley, D.V. McCalley, J. Chromatogr. A 1216 (2009) 3961.
[44] K. Kaczmarski, J. Kostka, W. Zapała, G. Guiochon, J. Chromatogr. A 1216 (2009) 6560.